View metadata, citation and similar papers at core.ac.uk

brought to you by CORE

provided by ZORA

University of Zurich[UZH]

Zurich Open Repository and Archive
University of Zurich
Main Library
Strickhofstrasse 39
CH-8057 Zurich
www.zora.uzh.ch

Year: 2020

The FDA-approved drug Nelfinavir inhibits lytic cell-free, but not cell-associated non-lytic transmission of human adenovirus

Georgi, Fanny ; Andriasyan, Vardan ; Witte, Robert ; Murer, Luca ; Hemmi, Silvio ; Yu, Lisa ; Grove, Melanie ; Meili, Nicole ; Kuttler, Fabien ; Yakimovich, Artur ; Turcatti, Gerardo ; Greber, Urs F

Abstract: Adenoviruses (AdVs) are prevalent and give rise to chronic and recurrent disease. The human AdV (HAdV) species B and C, such as HAdV-C2, C5 and B14, cause respiratory disease, and constitute a health threat for immuno-compromised individuals. HAdV-Cs are well known for lysing cells, owing to the E3 CR1- -encoded adenovirus death protein (ADP). We previously reported a high-throughput image-based screening frame-work and identified an inhibitor of HAdV-C2 multi-round infection, Nelfinavir mesylate. Nelfinavir is the active ingredient of Viracept, an FDA-approved inhibitor of the human immuno-deficiency virus (HIV) aspartyl protease, and used to treat acquired immuno-deficiency syndrome (AIDS). It is not effective against single round HAdV infections. Here, we show that Nelfinavir inhibits the lytic cell-free transmission of HAdV, indicated by the suppression of comet-shaped infection foci in cell culture. Comet-shaped foci occur upon convection-based trans-mission of cell-free viral particles from an infected cell to neighbouring uninfected cells. HAdV lacking ADP was insensitive to Nelfinavir, but gave rise to comet-shaped foci indicating that ADP enhances but is not required for cell lysis. This was supported by the notion that HAdV-B14 and B14p1 lacking ADP were highly sensitive to Nelfinavir, although HAdV-A31, B3, B7, B11, B16, B21, D8, D30 or D37 were less sensitive. Conspicuously, Nelfinavir unco-vered slow-growing round-shaped HAdV-C2 foci, independent of neutralizing antibodies in the medium, indicative of non-lytic cell-to-cell transmission. Our study demonstrates the repurposing potential of Nelfinavir with post-exposure efficacy against different HAdVs, and describes an alternative non-lytic cell-to-cell transmission mode of HAdV.

DOI: https://doi.org/10.1128/aac.01002-20

Posted at the Zurich Open Repository and Archive, University of Zurich
ZORA URL: https://doi.org/10.5167/uzh-188547
Journal Article
Accepted Version

The following work is licensed under a Creative Commons: Attribution 4.0 International (CC BY 4.0) License.

Originally published at:
Georgi, Fanny; Andriasyan, Vardan; Witte, Robert; Murer, Luca; Hemmi, Silvio; Yu, Lisa; Grove, Melanie; Meili, Nicole; Kuttler, Fabien; Yakimovich, Artur; Turcatti, Gerardo; Greber, Urs F (2020).

The FDA-approved drug Nelfinavir inhibits lytic cell-free, but not cell-associated non-lytic transmission of human adenovirus. Antimicrobial Agents and Chemotherapy, 64(9):e01002-20.
DOI: https://doi.org/10.1128/aac.01002-20

AAC Accepted Manuscript Posted Online 29 June 2020
Antimicrob. Agents Chemother. doi:10.1128/AAC.01002-20
Copyright © 2020 Georgi et al.
This is an open-access article distributed under the terms of the Creative Commons Attribution 4.0 International license.

Accepted Manuscript Posted Online
Antimicrobial Agents and Chemotherapy
AAC
Antimicrobial Agents and Chemotherapy

The FDA-approved drug Nelfinavir inhibits lytic cell-free, but not cell-associated non-lytic transmission of human adenovirus

Fanny Georgi [1], Vardan Andriasyan [1], Robert Witte [1], Luca Murer [1], Silvio Hemmi [1], Lisa Yu [1], Melanie Grove [1], Nicole Meili [1], Fabien Kuttler [2], Artur Yakimovich [1,3,4], Gerardo Turcatti [2], Urs F Greber [1,5]

[1] Department of Molecular Life Sciences, University of Zurich, Zurich, Switzerland
[2] Biomolecular Screening Facility, School of Life Sciences, Ecole Polytechnique Fédérale de Lausanne, Lausanne, Switzerland
[3] MRC Laboratory for Molecular Cell Biology, University College London, London, United Kingdom
[4] Artificial Intelligence for Life Sciences CIC, 40 Gowers walk, London, E1 8BH, United Kingdom
[5] Corresponding author: urs.greber@mls.uzh.ch

Abstract

Adenoviruses (AdVs) are prevalent and give rise to chronic and recurrent disease. The human AdV (HAdV) species B and C, such as HAdV-C2, C5 and B14, cause respiratory disease, and constitute a health threat for immuno-compromised individuals. HAdV-Cs are well known for lysing cells, owing to the E3 CR1-β-encoded adenovirus death protein (ADP). We previously reported a high-throughput image-based screening framework and identified an inhibitor of HAdV-C2 multi-round infection, Nelfinavir mesylate. Nelfinavir is the active ingredient of Viracept, an FDA-approved inhibitor of the human immuno-deficiency virus (HIV) aspartyl protease, and used to treat acquired immunodeficiency syndrome (AIDS). It is not effective against single round HAdV infections. Here, we show that Nelfinavir inhibits the lytic cell-free transmission of HAdV, indicated by the suppression of comet-shaped infection foci in cell culture. Comet-shaped foci occur upon convection-based transmission of cell-free viral particles from an infected cell to neighbouring uninfected cells. HAdV lacking ADP was insensitive to Nelfinavir, but gave rise to comet-shaped foci indicating that ADP enhances but is not required for cell lysis. This was supported by the notion that HAdV-B14 and B14p1 lacking ADP were highly sensitive to Nelfinavir, although HAdV-A31, B3, B7, B11, B16, B21, D8, D30 or D37 were less sensitive. Conspicuously, Nelfinavir uncovered slow-growing round-shaped HAdV-C2 foci, independent of neutralizing antibodies in the medium, indicative of non-lytic cell-to-cell transmission. Our study demonstrates the repurposing potential of Nelfinavir with post-exposure efficacy against different HAdVs, and describes an alternative non-lytic cell-to-cell transmission mode of HAdV.

Downloaded from http://aac.asm.org/ on July 13, 2020 by guest

Accepted Manuscript Posted Online

Antimicrobial Agents and Chemotherapy

AAC

Antimicrobial Agents and Chemotherapy

Downloaded from http://aac.asm.org/ on July 13, 2020 by guest

Introduction

Adenovirus (AdV) was first described in 1953 by Rowe and co-workers as a cytopathologic agent isolated from human adenoids (1). More than 100 human AdV (HAdV) genotypes have since been characterized by molecular genetics or serology and grouped into seven species (2, 3). HAdV species A, F and G replicate in the gastrointestinal tract, B, C and E in the respiratory organs, and B and D in conjunctival cells of the eyes. Species B members have a broad tropism, including kidney and cells of the hematopoietic lineage (4–6). HAdV-caused illness can range from asymptomatic to lethal, especially in immunocompromised individuals (7–9). HAdV outbreaks are frequent in military training camps, but also nursing homes, as recorded in recurrent outbreaks of HAdV-E4 and HAdV-B7 (5, 10–13). To counter the disease burden, an oral HAdV-E4/B7 vaccine was reintroduced, leading to a sharp decline in adenoviral disease among military recruits (5, 14, 15). In addition to recurrent HAdV outbreaks, novel HAdV variants emerge, some of them causing pneumonia and death of elderly with chronic diseases. One of these emerging HAdVs is the HAdV-B14 variant 14p1, also known as 14a (16–20). Furthermore, AdVs have a potential for zoonotic transmission (21). Cross-species infections to humans from either non-human primates or psittacine birds have been reported from the USA and China, respectively (22, 23). Despite the high prevalence (5, 24–26) and the broad use of AdV as gene therapy vectors (27) as well as oncolytic viruses (28, 29) no FDA-approved specific anti-HAdV treatment is available to date. Clinically, HAdV infections are treated with Ribavirin, Cidofovir, or more recently, Brincidofovir, which all inhibit viral DNA replication (30, 31).

HAdV particles have been well characterized. They have a double-stranded DNA genome of ~36 kilo base pairs (kbp) packaged into an icosahedral capsid of about 90 nm in diameter (32–35). HAdV-C2 and C5 replication cycle has been extensively studied including entry, uncoating, replication, assembly and egress from the infected cell (36–50). HAdV-C infects cells by binding to the coxsackievirus adenovirus receptor (CAR) and integrin co-receptors, followed by receptor-mediated endocytosis, endosomal lysis and microtubule-motor driven transport to the nucleus, where it uncoats DNA and delivers the DNA into the nucleus (38, 51–62). The first viral protein expressed is E1A, a multifunctional intrinsically disordered protein controlling the transcriptional activity of all AdVs, as well as many cellular promoters, thereby affecting the cell cycle, differentiation, transformation and apoptosis (63–68). Viral early proteins besides E1A mediate immune escape, block activation of pro-apoptotic pathways and form nuclear viral DNA replication compartments. Late viral proteins give rise to mature progeny virions upon limited proteolysis of capsid proteins by the viral cysteine protease L3/p23 (69–71). Mature HAdV progeny is released upon rupture of the nuclear envelope and plasma membrane, which facilitates rapid viral dissemination and plaque formation *in vitro* (72–74). The convection forces in the medium give rise to comet-shaped infection foci in cell cultures (72). Foci of infected cells are also found in tissue, such as rat liver upon intravenous inoculation of HAdV-C5 (75). Accordingly, acute HAdV infections trigger an inflammatory response, as shown in airways or conjunctiva of susceptible animals (2, 76). In contrast to lytic virus transmission, direct cell-to-cell transmission leads to round plaques, as shown with vaccinia virus (77–80).

Accepted Manuscript Posted Online

The mechanisms of virus transmission are highly virus-specific. They comprise non-lytic pathways involving the secretory-endocytic circuits, multi-vesicular or autophagic membrane processes, cellular protrusions, or transient breaches of membrane integrity (80–84). In contrast, lytic egress pathways further involve the destabilization of cellular membranes by viral and host factors, often tuned by the cytoskeleton (37, 85–88). HAdV-C2 controls lytic cell death by the adenovirus death protein (ADP), also known as 11.6K, as concluded from genetic and overexpression studies (73, 74). ADP is a type III membrane protein transcribed from the CR1-β region in the immuno-regulatory E3a locus. All HAdV-C members harbour homologous E3a CR1-β sequences (e.g. 10.5K in HAdV-C5). Other HAdV species differ in their E3 region, however (89–91). The N-terminus of ADP is lumenal and the C-terminus protrudes into the cytosol (92). Following post-translational modifications, ADP is transported to the inner nuclear membrane, where the N-terminus is intruding into the nucleus (93). At late stages, when capsid assembly in the nucleus has commenced ADP expression is boosted (94, 95). The mechanism of host cell lysis is still unknown, although necrosis-like, autophagic and caspase activities have been implicated (96–99).

Here, we report that Nelfinavir mesylate (Nelfinavir in short) is an effective inhibitor of HAdV lytic egress. The identification process of Nelfinavir is described in an accompanying paper using an imaging-based, high content screen of the Prestwick Chemical Library (PCL) comprising 1,280 mostly clinical or preclinical compounds (100, 101). Nelfinavir is the off-patent active pharmaceutical ingredient of Viracept, FDA-approved, which inhibits the human immuno-deficiency virus (HIV) protease (102). The work here documents the repurposing potential of Nelfinavir, which is effective against a spectrum of HAdV types in a post exposure manner. Nelfinavir is partly, but not exclusively, active against ADP-encoding HAdV types, and uncovers the appearance of round-shaped plaques, which arise upon non-lytic cell-to-cell viral transmission.

Antimicrobial Agents and Chemotherapy
AAC
Antimicrobial Agents and Chemotherapy
Downloaded from http://aac.asm.org/ on July 13, 2020 by guest

Accepted Manuscript Posted Online

Materials and Methods

Viruses

HAdV-C2-dE3B-GFP was previously described (72) (GenBank accession number MT277585). The virus was generated by exchange of the viral E3b genome region with a reporter cassette harbouring the enhanced green fluorescent protein (GFP) under a constitutively active cytomegalovirus (CMV) promoter. It was grown in A549 cells and purified by double CsCl gradient centrifugation (103). Aliquots supplemented with 10% (v / v) glycerol were stored at -80°C. HAdV-C2-dE3B-GFP was found to be homogeneous by SDS-PAGE and negative-stain analyses in transmission electron microscopy (EM). Recombinant HAdV-C2-dE3B-GFP-dADP was generated using homologous recombination according to the Warming recombineering protocols (104, 105). For a detailed protocol, see Supplementary methods. HAdV-C2-dE3B-GFP-dADP was plaque-purified and amplified, followed by two rounds of CsCl purification (106). Aliquots containing 10% (v / v) glycerol were stored at -80°C. HAdV-C2-dE3B-GFP-dADP was found to be homogeneous in SDS-PAGE and negative-stain analyses by transmission EM. Lack of ADP expression was confirmed by Western immunostaining using the rabbit α-HAdV-C2-ADP_{78-93} antibody, obtained from William Wold and Ann Tollefson (Saint-Louis University, Saint-Louis, USA) (107).

HAdV types A31, B7, B11, B14a, B16, B34, C1, C6, D8, D30 and D37 were kindly provided by the late Thomas Adrian (Hannover Medical School, Germany) and were verified by DNA restriction analysis (108, 109). HAdV types B14 (19, 20) and B21a, isolate LRTI-6 (110) were kindly provided by Albert Heim (Hannover Medical School, Germany). HAdV-B3-pIX-FS2A-GFP and B35-pIX-FS2A-GFP contain an enhanced GFP open reading frame (ORF) genetically fused to the downstream end of the HAdV pIX gene using an autocleavage FS2A sequence (111–113). rec700 (114) and dl712 (115) were obtained from William Wold (Saint-Louis University, Saint-Louis, USA). rec700 is a recombinant HAdV-C5 containing C2 sequences from nucleotide -236 to 2437 of the E3 transcription unit, and comprises the C2 E3a ORFs 12.5K, 6.7K, 19K and ADP, as well as major parts of the E3b ORF RIDα (10.4K protein) (116). Mouse adenovirus (MAdV)-1-pIX-FS2A-GFP and MAdV-3-pIX-FS2A-GFP were constructed as described (117, 118). HAdV-C2 and C5 were obtained from Maarit Suomalainen (University of Zurich, Switzerland). HSV-1-CMV-GFP is a recombinant HSV-1 strain SC16 containing a CMV enhancer/promoter-driven enhanced GFP expression cassette in the US5 (gJ) locus (119) and was kindly provided by Cornel Fraefel (University of Zurich, Switzerland). HSV-1-CMV-GFP was propagated in Vero cells and purified by sucrose sedimentation as described in (120, 121). All viruses were stored in small aliquots containing 10% (v / v) glycerol at -80°C.

Cell lines

A549 (human adenocarcinomic alveolar basal epithelium, CCL-185), HeLa (human epithelial cervix carcinoma, CCL-2) and HBEC (HBEC3-KT, normal human bronchial epithelium, CRL-4051) cells were obtained from the American Type Culture Collection (ATCC, Manassas, USA). HCE (normal human corneal epithelium) cells were obtained from Karl Matter (University College London, UK). CMT93 (mouse rectum carcinoma) cells were obtained from Susan

Antimicrobial Agents and Chemotherapy
AAC
Antimicrobial Agents and Chemotherapy
Downloaded from http://aac.asm.org/ on July 13, 2020 by guest

Accepted Manuscript Posted Online

Compton, Yale School of Medicine, USA. A549, HeLa, HCE and CMT-93 cell cultures were maintained in high glucose DMEM (Thermo Fisher Scientific, Waltham, USA) containing 7.5% (v / v) FCS (Invitrogen, Carlsbad, USA), 1% (v / v) L-glutamine (Sigma-Aldrich, St. Louis, USA) and 1% (v / v) penicillin streptomycin (Sigma-Aldrich, St. Louis, USA) and subcultured following phosphate-buffered saline (PBS) washing and trypsinisation (Trypsin-EDTA, Sigma-Aldrich, St. Louis, USA) bi-weekly. HBEC cells were maintained in endothelial-basal medium (ATCC, Manassas, USA) and passaged 1:1 weekly following PBS washing and trypsinisation. Cell cultures were grown at standard conditions (37°C, 5% CO_2, 95% humidity) and passage number was limited to 20. Respective supplemented medium is referred to as supplemented medium.

Compounds

Nelfinavir mesylate (CAS number 159989-65-8) powder was obtained from MedChemExpress LLC (Monmouth Junction, USA and Selleck Chemicals, Houston, USA). Compound was dissolved in DMSO (Sigma-Aldrich, St. Louis, USA) at 100 mM and kept at -80°C or -20°C for long-term or working storage, respectively.

Cellular impedance measurement

Impedance-based assays were performed using the xCELLigence system (Roche Applied Science and ACEA Biosciences) as described previously (122, 123) according to the manufacturer's instructions (124) in cell culture environment (37°C, 5% CO_2, 95% humidity) in duplicates. The 16-well E plates have a gold-plated sensor array embedded in their glass bottom by which the electrical impedance across each well bottom is measured. The impedance per well, termed cell index (CI), is recorded as a dimensionless quantity. The background CI was assessed following the addition of 50 µl supplemented medium to each well and equilibration in the incubation environment. After 30 min equilibration, 9,000 A549 ATCC cells in 50 µl supplemented medium were added per well and measurement was started.

For the quantification of Nelfinavir toxicity, 50 µl of supernatant were removed 18 h later and replaced by 2-fold concentrated Nelfinavir or DMSO solvent as the control dilution in supplemented medium (final Nelfinavir concentration 0.4-100 µM in 100 µl / well). The control was supplemented medium. Impedance was recorded every 15 min over 5 days. TC_{50} indicates the concentration of Nelfinavir, which caused 50% impedance reduction compared to the solvent-treated cells. TC_{50} was calculated by non-linear regression of solvent-normalized CI over the concentration of Nelfinavir.

For the quantification of Nelfinavir effects on the cytopathogenicity of HAdV-C2-dE3B-GFP compared to HAdV-C2-dE3B-GFP-dADP infection, 50 µl supernatant were removed 18 h later and replaced with Nelfinavir- and virus-supplemented medium. 25 µl of a 4-fold concentrated Nelfinavir (final concentration 0.4-100 µM) or corresponding DMSO solvent control dilution (final concentration 1%) in supplemented medium or supplemented medium only were added to 50 µl medium containing cells. Additionally, 25 µl of a 4-fold concentrated virus stock dilution were added (final inoculum $1.68*10^6$ viral particle(s) (VP) / well HAdV-C2-dE3B-GFP and $2.68*10^6$ VP/ well HAdV-C2-dE3B-dADP, corresponding to ~30 plaque forming unit(s) (pfu) / well. The

Downloaded from http://aac.asm.org/ on July 13, 2020 by guest

Antimicrobial Agents and Chemotherapy

AAC

Antimicrobial Agents and Chemotherapy

Accepted Manuscript Posted Online

delay of infection-induced cytotoxicity was calculated as time point at which the CI of the infected cells had decreased by 50% relative to its maximum. Data analysis was performed using GraphPad (GraphPad Software, Inc, version 8.1.2), and curve fitting was performed using three-parameter [inhibitor] vs. response nonlinear regression.

Fluorescence-based plaque forming assay

Per 96-well, 15,000 A549, 10,000 HeLa ATCC, 30,000 HBEC, 30,000 HCE or 30,000 CMT-93 cells were seeded in 100 µl of the respective supplemented medium and allowed to settle for 1 h at room temperature (RT) prior to cell culture incubation at 37°C, 5% CO_2, 95% humidity. The following day, the medium was replaced by 50 µl of the respective virus stock dilution giving rise to 5 to 50 plaques per 96-well. 50 µl Nelfinavir to obtain 0.1 to 50 µM final concentration or DMSO solvent control was also added, both in supplemented medium. For each experiment, a non-infected, treated control was performed. For uphill plaque assays, medium volume was increased to 150 µl with identical virus and drug concentrations. For wash-in / wash-out experiments, virus was incubated on the cells in supplemented medium for 1 h at 37°C, cells were washed with PBS and 100 µl drug dilution in supplemented medium was added. All experiments were performed in four technical replicates or as indicated. Cells were incubated at standard cell culture conditions. At the indicated time post infection (pi), the cells were fixed and the nuclei stained for 1 h at RT by addition of 33 µl 16% (w / v) para-formaldehyde (PFA) and 4 µg / ml Hoechst 33342 (Sigma-Aldrich, St. Louis, USA) in PBS. Cells were washed three times with PBS and stored in PBS supplemented with 0.02% N_3 for infections with viruses harbouring a GFP transgene. For wild type (wt) viruses, cells were quenched in PBS supplemented with 50 mM NH_4Cl, permeabilized using 0.2% (v / v) Triton-X100 in PBS and blocked with 0.5% (w / v) BSA in PBS. Cells were incubated with 381.7 ng / ml mouse α-HAdV hexon protein antibody (Mab8052, Sigma-Aldrich, St. Louis, USA) and subsequently stained using 2 µg / ml goat α-mouse-AlexaFluor594 (A21203 or A32742, Thermo Fisher Scientific, Waltham, USA). Plates were imaged on either an IXM-XL or IXM-C automated high-throughput fluorescence microscope (Molecular Devices, San Jose, USA) using a 4x objective at widefield mode. Hoechst staining was recorded in DAPI channel, FITC / GFP channel for viral GFP and TRITC / Texas red channel for immunofluorescence hexon staining.

Therapeutic index measurement

The infection phenotype for each well was quantified using Plaque2.0 (101). The number of plaques was determined based on the infection signal (viral GFP or hexon immunofluorescence staining). Nuclei stained with Hoechst were segmented by CellProfiler (125). Infected nuclei were classified based on the median infection signal per nucleus in CellProfiler. Data were plotted and EC_{50} (infected and treated cells), TC_{50} (non-infected, treated cells), as well as the corresponding standard error (SE) determined using curve fitting in GraphPad (GraphPad Software, Inc, version 8.1.2) using three-parameter [inhibitor] vs. response nonlinear regression. Mean TI_{50} was calculated as EC_{50} / TC_{50} ratio of the means. The TI_{50} SE was calculated by error propagation.

Quantification of viral protein expression

Downloaded from http://aac.asm.org/ on July 13, 2020 by guest

Antimicrobial Agents and Chemotherapy
AAC
Antimicrobial Agents and Chemotherapy

Accepted Manuscript Posted Online

Infection, HAdV hexon immunofluorescence staining, and imaging were performed in technical quadruplicates, as described under Microscopic plaque assay. Single nuclei (Hoechst) were segmented using CellProfiler (125). Median GFP and hexon signals per nucleus were measured, and infected nuclei classified using the median GFP or hexon signals per nucleus. Subsequently, mean and standard deviation (SD) over all infected nuclei per well were calculated in R version 3.3.2 (126). Data were plotted in GraphPad (GraphPad Software, Inc, version 8.1.2).

Transmission electron microscopy

A549 ATCC cells grown on Alcian Blue-treated cover slips were infected with HAdV-C2-dE3B-GFP in supplemented medium with 0, 1.25 or 3 µM Nelfinavir and cultured for 40 h at standard cell culture conditions. The samples were washed with ice-cold 0.1 M cacodylate buffer (pH 7.4) and fixed at 4°C in 0.1 M ice-cold cacodylate buffer (pH 7.4), supplemented with 2.5% (v / v) glutaraldehyde and 0.5 mg / ml ruthenium red for 1 h. Cells were washed with 0.1 M cacodylate buffer (pH 7.4) and post-fixed at RT in 0.05 M cacodylate buffer (pH 7.4) supplemented with 0.5% (v / v) OsO_4 and 0.25 mg / ml ruthenium red for 1 h. Following washing with 0.1 M cacodylate buffer (pH 7.36) and H_2O, the samples were incubated in 2% (v / v) uranyl acetate at 4°C over night (ON). The samples were dehydrated in acetone and embedded in Epon as described in (127). 85 nm slices were obtained (Leica Ultracut UCT, Leica, Wetzlar, Germany) and stained with uranyl acetate.

HAdV-C5 virus production in presence of Nelfinavir

HAdV-C5 was amplified in the medium containing 0, 1.25 or 3 µM Nelfinavir for 4 days. Cells were harvested and disrupted by three freeze / thaw cycles. The cell debris was removed by Freon extraction and mature full HAdV virions were purified by two rounds of CsCl gradient ultracentrifugation (106). Protein concentration was determined by BCA assay (Pierce BCA Protein Assay Kit, Thermo Fisher Scientific, Waltham, USA). For long-term storage, virus stocks were supplemented with 10% (v / v) glycerol and kept at -80°C.

Negative staining electron microscopy

Double CsCl gradient-purified HAdV particles were adhered to Collodion and 2% (v / v) amyl acetate film-covered grids (300 mesh Formvar/carbon-supported copper support films, Electron Microscopy Sciences, Hatfield, USA). Viral particles were negatively stained with 2% (v / v) uranyl acetate and viewed on a transmission electron microscope (Philips CM100, Philips, Amsterdam, Netherlands) at 100 kV. Images were acquired using a CCD camera (Orius SC1000 with 4,000 x 2,600 pixels, Gatan, Pleasanton, USA).

Western blot analysis of HAdV protease activity

Double CsCl-purified grown in presence / absence of Nelfinavir (HAdV-C5$^{\pm Nelfinavir}$) stocks and size standard (PageRuler plus, Thermo Fisher Scientific, Waltham, USA) were size-separated on 12% acrylamide gel under reducing conditions and transferred to a PVDF membrane. HAdV proteins were detected using the following primary antibodies: 1:10,000 R72 rabbit α-fiber (128),

Antimicrobial Agents and Chemotherapy
AAC
Antimicrobial Agents and Chemotherapy
Downloaded from http://aac.asm.org/ on July 13, 2020 by guest

Accepted Manuscript Posted Online

1:1,000 rabbit α-pVI/VI (51), 1:1,000 R3 rabbit α-pVII/VII (Ulf Pettersson of Uppsala University) and visualized using a goat α-rabbit-HRP (7074, Cell Signaling Technology, Danvers, USA) and ECL Prime Western Blotting Detection Reagent (GE Health Care, Pittsburgh, USA). The membranes were luminescence imaged on an Amersham Imager 680 (GE Health Care, Pittsburgh, USA).

Determination of nuclear size

Infection and Nelfinavir treatment of A549 cells were performed as described under Microscopic plaque assay with a cell seeding density of 15,000 cells / well. Wells were imaged with IXM-C automated high-throughput fluorescence microscope (Molecular Devices, San Jose, USA) using a 40x objective (NA 0.95) at confocal mode (62 µm pinhole). DAPI channel was acquired for nuclear Hoechst staining, FITC / GFP channel was acquired for viral GFP, TRITC / Texas red channel was acquired for immunofluorescence ADP staining and Cy5 channel was acquired for NHS-ester signal. 30 z steps with 0.5 µm step size were acquired for each channel and maximal projections were calculated. Image analysis was performed using CellProfiler (125). Nuclei areas were segmented based on thresholded Hoechst signal. Infected cells were classified based on a fixed threshold for median nuclear GFP intensity. Data processing was performed in R version 3.3.2 (126). Statistical analysis was performed in GraphPad (GraphPad Software, Inc, version 8.1.2) using the non-parametric Kolmogorov-Smirnov test.

Cell binding assay of virus

A549 cells were seeded at 7,500 cells per 96-well in full DMEM and allowed to attach over night at standard cell culture conditions. The next day, the medium was replaced by $3*10^8$ VP/ well of double CsCl-purified HAdV-C5$^{\pm Nelfinavir}$ virus stocks in 100 µl ice-cold supplemented medium and kept on ice for 30 min. Following a 15 min entry phase under standard cell culture conditions the cells were fixed and the nuclei stained for 1 h at RT by addition of 33 µl 16% PFA and 4 µg / ml Hoechst 33342 (Sigma-Aldrich, St. Louis, USA) in PBS. Following the above described immuno-fluorescence staining procedure, the cell-bound HAdV virions were stained using 9C12 mouse α-hexon (developed by Laurence Fayadat and Wiebe Olijve, obtained from Developmental Studies Hybridoma Bank developed under the auspices of the National Institute of Child Health and Human Development and maintained by the University of Iowa, Iowa City, USA) (129) and goat α-mouse AlexaFluor488 (A11029, Thermo Fisher Scientific, Waltham, USA). Total area was identified by Alexa-Fluor647 NHS ester staining (A20006, Thermo Fisher Scientific, Waltham, USA). Max projections of confocal z-stacks (25 z steps spaced 1 µm) were acquired on a SP5 resonant APD (Leica, Wetzlar, Germany) at 1.7x zoom using a 63x glycerol objective (numerical aperture 1.4).

Assessment of HAdV infectivity of HAdV-C5$^{\pm Nelfinavir}$

Fifteen thousand A549 cells were seeded per 96-well in full DMEM and allowed to attach over night at standard cell culture conditions. The next day, the medium was replaced by double CsCl-purified HAdV-C5$^{\pm Nelfinavir}$ virus stocks at 50 to 0.001 pg / well of BCA-based viral protein concentration and incubated at standard cell culture conditions. Cells were fixed at 52 hpi, stained for HAdV hexon expression and imaged following the procedure described under

Antimicrobial Agents and Chemotherapy
AAC
Antimicrobial Agents and Chemotherapy
Downloaded from http://aac.asm.org/ on July 13, 2020 by guest

Accepted Manuscript Posted Online

Image-based plaque assay. Images were quantified using Plaque2.0 (101). Nuclei were segmented based on Hoechst signal. Infected cells were segmented based on hexon immunofluorescence staining signal.

Egress assay

A549 cells were seeded at 480,000 cells per 6-well in full DMEM and infected at 1,100 pfu HAdV-C2-dE3B-GFP per well the next day. Following 1 h of warm incubation, the supernatant was removed, and cells were washed with PBS and detached by trypsin digestion. Infected cells were centrifuged and resuspended in fresh medium to remove any unbound input virus and seeded at 180,000 cells / 12-well in medium supplemented with 1.25, 3 or 10 µM Nelfinavir or equivalent amounts of DMSO solvent control. At the indicated times pi, the supernatant was harvested and cleared by centrifugation. 200 µl PBS / well was added to the infected monolayer. Cells were disrupted by three freeze / thaw cycles and freon extraction was performed. Supernatant and cell lysate were stored at 4°C until titration on naive A549 cells. PFA-fixed, Hoechst-stained cells were imaged at 44 hpi using a 4x objective (NA 0.20) on an epifluorescence IXM-XL (Molecular Devices, San Jose, USA). GFP-positive infected cells were classified based on median nuclear GFP intensity using automated image analysis by CellProfiler (125).

Quantification of infectious progeny production

Four hundred and eighty thousand A549 cells were seeded per 6-well dish and inoculated with 1,100 pfu HAdV-C2-dE3B-GFP / well for 1 h at 37°C, washed with PBS and detached by trypsin digestion. Infected cells were centrifuged and resuspended in fresh medium to remove any unbound input virus. Cells were seeded at 180,000 cells / 12-well in medium supplemented with 1.25, 3 or 10 µM Nelfinavir or the respective DMSO solvent control. Viral progeny in the cell monolayer and supernatant was harvested at the indicated time pi by three freeze / thaw cycles. The lysates were cleared by centrifugation and stored at 4°C until titration on naive A549 cells. PFA-fixed, Hoechst-stained cells were imaged at 44 hpi using a 4x objective on an epifluorescence IXM-XL (Molecular Devices, San Jose, USA). GFP-positive infected cells were classified based on median nuclear GFP intensity using automated image analysis by CellProfiler (125). The yield per 12-well was extrapolated by linear regression of the number of infected cells per µl of harvested whole well lysate using GraphPad (GraphPad Software, Inc, version 8.1.2).

Quantification of the antiviral potency of Nelfinavir

Infection was performed as described under Microscopic plaque assay. Cells were incubated with an inoculum ranging between 10 - 2,560 pfu / well HAdV-C2-dE3B-GFP for 1 h at 37°C. Cells were washed with PBS and 100 µl DMEM phenol-free medium (Thermo Fisher Scientific, Waltham, USA), supplemented with 1% penicillin streptomycin (Sigma-Aldrich, St. Louis, USA), 1% L-glutamine (Sigma-Aldrich, St. Louis, USA), 7.5% FBS (Invitrogen, Carlsbad USA), 1% non-essential amino acids (Sigma-Aldrich, St. Louis, USA), 1% 100 mM sodium pyruvate (Thermo Fisher Scientific, Waltham, USA), 0.25 ng / ml Hoechst 33342 (Sigma-Aldrich, St. Louis, USA) and 1 µg / ml propidium iodide (PI, Molecular Probes, Eugene, USA). Plates were

Antimicrobial Agents and Chemotherapy
AAC
Antimicrobial Agents and Chemotherapy
Downloaded from http://aac.asm.org/ on July 13, 2020 by guest

Accepted Manuscript Posted Online

imaged at the indicated times pi on an IXM-C automated high-throughput fluorescence microscope (Molecular Devices, San Jose, USA) using a 40x objective (NA 0.95) at confocal mode (62 µm pinhole). DAPI channel was acquired for nuclear Hoechst staining, FITC / GFP channel was acquired for viral GFP and Cy5 channel was acquired for PI signal. 30 z steps with 0.5 µm step size were acquired for each channel and maximal projections were calculated.

Morphological plaque characterization

Plaques were segmented in Plaque2.0 (101) and plaque region eccentricity was measured as fraction of the distance between the two focal points of the ellipse divided by the length of the major axis. Only plaque regions consisting of at least five infected cells (≥6,000 px^2) with a centroid located 600 px from the well rim were considered to exclude spatial limitations. Plaque roundness was calculated as 1- eccentricity (Equation 1).

$$\text{roundness} = 1 - \frac{4\pi * \text{area}}{\text{perimeter}^2} \qquad \text{Equation 1}$$

Statistical analysis was performed in GraphPad (GraphPad Software, Inc, version 8.1.2) using the non-parametric Kolmogorov-Smirnov test.

Confocal microscopy of ADP localization

Infection and immunofluorescence stainings were performed as described under Microscopic plaque assay with a cell seeding density of 3,000 cells / well. Cells were incubated with 1:1,000 rabbit α-HAdV-C2-$ADP_{87\text{-}101}$ antibody (107) and subsequently stained using donkey α-rabbit-AlexaFluor594 (21207, Thermo Fisher Scientific, Waltham, USA) and 0.2 µg/ml NHS ester (Life Technologies, Carlsbad, USA) for whole cell outline. Plates were imaged on an IXM-C automated high-throughput fluorescence microscope (Molecular Devices, San Jose, USA) using a 40x objective (NA 0.95) at confocal mode (62 µm pinhole). DAPI channel was acquired for nuclear Hoechst staining, FITC / GFP channel was acquired for viral GFP, TRITC / Texas red channel was acquired for immunofluorescence ADP staining and Cy5 channel was acquired for NHS ester signal. 30 z steps with 0.5 µm step size were acquired for each channel and maximal projections were calculated. Image analysis was performed using CellProfiler (125). Nuclei and whole cell areas were segmented based on thresholded Hoechst and NHS ester signal, respectively. Nuclear rim was defined as 10 pixel-wide area around the nuclear border. Infected cells were classified based on the whole cell 5% quantile GFP intensity. Whole cell and nuclear rim mean TRITC / Texas red (detecting ADP) intensities as well as whole cell 5-pixel granularity per infected cell were normalized by the according mean over all infected cells of the solvent control. Data processing was performed in R version 3.3.2 (126). Statistical analysis was performed in GraphPad (GraphPad Software, Inc, version 8.1.2) using the non-parametric Kolmogorov-Smirnov test.

Western blot analysis of ADP processing

Four hundred and eighty thousand A549 cells were seeded per 6-well, incubated o/n and inoculated with HAdV-C2-dE3B-GFP at 22,000 pfu / well in 1.2 ml full DMEM supplemented with 0 to 10 µM Nelfinavir. Following 44 h of incubation in standard cell culture medium, cells were

Antimicrobial Agents and Chemotherapy
AAC
Antimicrobial Agents and Chemotherapy
Downloaded from http://aac.asm.org/ on July 13, 2020 by guest

Accepted Manuscript Posted Online

placed on ice and the supernatant was removed. The cells were washed twice with ice-cold PBS. Cells were lysed in 100 µl COS lysis buffer (20 mM Tris-HCl pH 7.4, 100 mM NaCl, 1 mM EDTA, 1% Triton X-100, 1 mM DTT, 25 mM β-Glycerophosphate disodium, 25 mM NaF, 1 mM Na_3VO_4, 1x protease inhibitors (Mini Complete, Roche, Basel, Switzerland) for 5 min on ice. Supernatant and washing PBS were collected and cells pelleted by centrifugation at 16,000 xg for 5 min at 4°C. Lysates were scraped off and used to resuspend the pelleted cells. Following another centrifugation, the supernatant was collected and stored at -20°C. Samples of 15 µl lysate were supplemented with SDS-containing loading buffer (0.35 M Tris-HCl pH 6.8, 0.28% SDS, 30 g / l DTT, 0.6 g / l bromophenol blue). Samples were denatured at 95°C for 5 min and proteins were separated on a denaturing 15% acrylamide gel. Proteins transferred to a PVDF membrane were detected with 1:1,000 of a rabbit α-HAdV-C2 ADP_{78-93} antibody (107) followed by goat α-rabbit-HRP (7074, Cell Signaling Technology, Danvers, USA). Protein bands were visualized using ECL Prime Western Blotting Detection Reagent (GE Health Care, Pittsburgh, USA) and luminescence imaged on an Amersham Imager 680 (GE Health Care, Pittsburgh, USA).

Neutralization of HAdV cell-free progeny

A549 cells were seeded at 15,000 cells per well of a 96-well-plate, incubated o/n and inoculated with HAdV-C2-dE3B-GFP at 34 pfu / well for 1 h at 37°C. Virus was removed and cells were washed with PBS, before 0.25 ng / ml Hoechst (Sigma-Aldrich, St. Louis, USA)-supplemented DMEM medium containing 1:12 HAdV-C2/5-neutralizing dog serum, kindly supplied by Anja Ehrhardt, University Witten/Herdecke, Germany (130), supplemented with 40% v / v glycerol), control goat serum (Thermo Fisher Scientific, Waltham, USA, supplemented with 40% v / v glycerol) or the corresponding volume glycerol only. Cells were imaged using a 4x objective (NA 0.20) on an epifluorescence IXM-XL microscope (Molecular Devices, San Jose, USA).

Crystal violet-stained plaques

Plaque shapes were also assessed by conventional crystal violet-stained plaque assay, performed in A549 cells in liquid supplemented DMEM medium. All infections were performed at 37°C, 95% humidity and 5% CO_2 atmosphere. At the indicated time pi, cells were fixed and stained for 60 min with PBS solution containing 3 mg / ml crystal violet and 4% PFA added directly to the medium from a 16% stock solution. Plates were de-stained in H_2O, dried and imaged using a standard 20 mega pixel phone camera under white light illumination.

Antimicrobial Agents and Chemotherapy
AAC
Antimicrobial Agents and Chemotherapy
Downloaded from http://aac.asm.org/ on July 13, 2020 by guest

Accepted Manuscript Posted Online

Results

Nelfinavir is a non-toxic, potent inhibitor of HAdV-C multicycle infection

An accompanying paper describes a full cycle, image-based screen of 1,278 out of 1,280 PCL compounds against HAdV-C2-dE3B-GFP, where Clopamide and Amphotericine B were excluded due to precipitation during acoustic dispension into the screening plates (100). The screen was conducted in adenocarcinomic human alveolar basal epithelial (A549) cells at 1.25 µM compound concentration, and identified Nelfinavir, Aminacrine, Dequalinium dichloride and Thonzonium bromide as hits (Supplementary Table 1). Nelfinavir (CAS number 159989-65-8), hereafter referred to as Nelfinavir, strongly inhibited plaque numbers at nanomolar concentrations, comparable to the known HAdV nucleoside analogue inhibitor 3'-deoxy-3'-fluorothymidine (DFT, Figure 1A, 1B). Dequalinium dichloride, Aminacrine and Thonzonium bromide were excluded from further analyses due to toxicity (100), and potential mutagenic effects (131). Long-term incubations of uninfected A549 cells with Nelfinavir up to 115 h showed median toxicity TC_{50} of 25.7 µM, as determined by cell impedance measurements using xCELLigence (Figure 1C). xCELLigence measures the impedance of electrical currents imposed by cell adherence to gold-plated microelectrodes implanted in culture wells. Impedance is expressed as cell index (CI), a unitless parameter proportional to the cell number, cell size, and cell adherence. For raw CI profiles, see Supplementary Figure 1A. CI measurements were consistent with presto-blue assays, and cell numbers determined by counting nuclei (Supplementary Table 1). This was in agreement with previous reports, and acceptable side effects in clinical use against HIV (102, 132). The therapeutic index 50 (TI_{50}) of Nelfinavir was 27.1 (Figure 1D), as determined by the ratio between the concentration yielding 50% loss of cell nuclei (TC_{50} = 10.01 µM) and the effective concentration yielding 50% inhibition of fluorescent plaque formation (EC_{50} = 0.37 µM). The data indicates that Nelfinavir is an effective, non-toxic inhibitor of HAdV-C2 multi-cycle infection.

Nelfinavir does not affect single round infection

We first tested if Nelfinavir affected viral protein production. HAdV-C2-dE3B-GFP-infected A549 cells were analysed for GFP under the immediate early CMV promoter, and the late protein hexon expressed after viral DNA replication at 46 hours post infection (hpi). Results indicate that Nelfinavir had no effect on GFP or hexon expression at the tested concentrations, while the formation of fluorescent plaques was completely inhibited (Figure 2A, and Figure 1D). This result was in agreement with the notion that Nelfinavir did not affect the replication of the HAdV-C5 genome, as determined by titration of cell-associated infectious particles (133). We next examined if Nelfinavir affected the formation of viral particles. Transmission electron microscopy (TEM) of HAdV-C2-dE3B-GFP-infected cells revealed large numbers of virions in the nuclei of Nelfinavir-treated and untreated cells (Figure 2B). This result was conforming with the observation that the nuclei of Nelfinavir-treated cells expanded in area over time, indistinguishable from control cells (Supplementary Figure 1B).

To test if Nelfinavir affected virion maturation, we analysed purified virions by SDS-PAGE and Western blotting against proteins pVI/VI and pVII/VII using previously characterized antibodies.

Antimicrobial Agents and Chemotherapy
AAC
Antimicrobial Agents and Chemotherapy
Downloaded from http://aac.asm.org/ on July 13, 2020 by guest

Accepted Manuscript Posted Online

There was no evidence for increase of precursor VI or VII (pVI or pVII) in HAdV-C5 from Nelfinavir-treated cells, in contrast to temperature-sensitive (ts) 1 particles, which lack the L3/p23 protease due to the point mutation P137L in p23 (134) (Figure 2C). This showed that Nelfinavir did not affect the proteolytic maturation of the virus by the L3/p23 cysteine protease. In accordance, purified HAdV-C5 from Nelfinavir-treated cells attached to naive A549 cells and gave rise to viral gene expression as effectively as control HAdV-C5 particles (Figures 2D, 2E). Together, these results indicate that Nelfinavir does not affect the production of infectious virions in single round infections.

Nelfinavir inhibits HAdV-C egress

We investigated the kinetics of HAdV-C2-dE3B-GFP production and the release to the supernatant. Supernatants and whole cell lysates of treated- and non-treated infected cells were harvested at different time points (Figure 3A). At 44 hpi, cell lysates of Nelfinavir and control cells contained similar infectivity, but did not yet release virus to the supernatant, as shown by titration on naive A549 cells. At 72 or 120 hpi, control cells, but not Nelfinavir-treated cells had released virus to the supernatant. Notably, the viral titer in the supernatant of control cells at 120 hpi was so high, that nearly all the cells in the indicator plates dissociated from the plates. The difference in infectious load was confirmed by titration of supernatants from separate time course experiments at three different concentrations of Nelfinavir (Figure 3B). At 7 dpi, a dosage of 1.25 μM reduced the total yield of infectious particles in the supernatant by three orders of magnitude, underscoring the potency of Nelfinavir to block the dissemination of HAdV-C-dE3B-GFP. Moreover, Nelfinavir limited HAdV-C2 transmission when added as late as 40 hpi (Figure 3C). These findings indicate that Nelfinavir impairs the egress of progeny from the host cell.

We next assessed the potency of the Nelfinavir against HAdV-C2 transmission by quantifying the number of nuclei, which normally decreases due to lytic virus replication. Nelfinavir (3 μM) robustly reduced the number of dead cells, and strongly reduced the number of infected cells up to 100 pfu / well (Figure 3D). Remarkably, HAdV-C2-dE3B-GFP formed delayed plaques in presence of Nelfinavir, starting at 4 dpi (Figures 3E, 3F). These late plaques showed a strikingly round morphology, which was calculated to be significantly different from the comet-shaped plaques early in infection of control cells (Figure 3G). The direction of the comet tail of lytic plaques can be aligned by tilting of the incubation plate (72). Thereby, the cell monolayer is positioned non-orthogonally to the vector of thermal convection flux of the liquid cell culture medium. While the direction of the comet-shaped plaques could be aligned using this method in the non-treated infections, the late Nelfinavir plaques remained mostly round (Supplementary Figures 2A-C). Moreover, there was no correlation between the size of the plaques and their roundness irrespective of Nelfinavir up to 7 dpi, demonstrating that the round plaques did not change morphology over time (Supplementary Figure 2D). Collectively, the data indicate that virus transmission in presence of Nelfinavir is not driven by the bulk current of cell free medium.

HAdV inhibition by Nelfinavir depends on ADP

ADP is expressed at high levels late in infection and enhances cell lysis (94, 135). To test if ADP was required for Nelfinavir inhibition of lytic spread, we generated an ADP-depleted HAdV-

Antimicrobial Agents and Chemotherapy
AAC
Antimicrobial Agents and Chemotherapy
Downloaded from http://aac.asm.org/ on July 13, 2020 by guest

Accepted Manuscript Posted Online

C2-dE3B-GFP mutant, HAdV-C2-dE3B-GFP-dADP. The mutant completely lacks ADP expression, as indicated by immunofluorescence and Western blot experiments (Supplementary Figure 3A, 3B). HAdV-C2-dE3B-GFP-dADP formed particles indistinguishable from HAdV-C2-dE3B-GFP, as indicated by negative stain EM (Supplementary Figure 3C). HAdV-C2-dE3B-GFP-dADP showed a delayed onset of plaque formation by about 1 day, compared to HAdV-C2-dE3B-GFP (Figure 4A). These data are in agreement with previous kinetic studies with the ADP deletion mutant HAdV-C dl712 (107) (see also Supplementary Figure 3A). HAdV-C2-dE3B-GFP-dADP plaques were comet-shaped, albeit their comet-heads appeared bigger and more dense (Figure 4A). While the parental virus was highly sensitive to Nelfinavir, HAdV-C2-dE3B-GFP-dADP required much higher concentrations of the compound to show inhibition of plaque formation (Figure 4B, Supplementary Table 2). In accordance, the ADP-deleted virus induced cell death independent of Nelfinavir, unlike the ADP-expressing virus, as concluded from cell impedance measurements with xCELLigence (Figure 4C, Supplementary Figures 3D, 3E). Finally, HAdV-C2-dE3B-GFP-dADP exhibited a strongly diminished separation of anti-viral efficacy from toxicity, as indicated by reduced TI_{50} values compared to the parental virus, for example 2.1 versus 66.8 with A549 cells, 8.9 versus 61.0 with HeLa cells, and 4.6 versus 55.2 with HBEC cells (Figure 4D). These effects were in agreement with similar experiments performed with the previously described ADP-knock out mutant dl712 and the parental rec700, an HAdV-C5/2 hybrid virus (135, 136). The data are shown in (Supplementary Figures 3F to 3H). Together, the results show that the selective antiviral effects of Nelfinavir are more cell-type dependent in case of HAdV lacking ADP than in ADP-expressing viruses, and the effects are comparatively small for viruses lacking ADP.

Finally, we performed immunofluorescence experiments with HAdV-C2-dE3B-GFP-infected A549 cells at 44 hpi (Figure 4E). Under non-perturbed conditions, ADP accumulated in cytoplasmic foci and the nuclear envelope. Nelfinavir treatment did not affect the overall ADP expression levels nor the amount of ADP in the nuclear periphery, including the nuclear envelope, but completely abolished the cytoplasmic ADP foci as indicated by granularity quantifications (Figure 4E, right graph). Intriguingly, Tollefson and co-workers observed earlier that ADP lacking lumenal O-glycosylation sites did not localize to large cytoplasmic granules and the corresponding HAdV-C mutant pm734.4 was non-lytic (107). We speculate that the localization of ADP in cytoplasmic organelles, such as Golgi compartments, where O-glycosylation occurs (137), could enhance the cell lytic function of ADP. Together, the data show that ADP is a major susceptibility factor for inhibition of HAdV-C infection spread by Nelfinavir.

A round non-lytic plaque phenotype in HAdV-C infection

Viruses are transmitted between cells by three major mechanisms, cell-free through the extracellular medium, directly from cell-to-cell, or in an organism by means of infected motile cells or fluid flow in blood or lymphoid vessels. This can result in far-reaching or mostly local virus dissemination (for a simplified cartoon, see Figure 5A). In cell culture, HAdV-C transmission from a lytic infected cell (staining PI-positive) yields comet-shaped infection foci due to convective passive mass flow in the cell culture medium (72, 101), consistent with lytic HAdV-C infection (74, 135). In accordance, neutralizing antibodies against HAdV-C2 added to the cell culture

Antimicrobial Agents and Chemotherapy
AAC
Antimicrobial Agents and Chemotherapy
Downloaded from http://aac.asm.org/ on July 13, 2020 by guest

Accepted Manuscript Posted Online

medium suppressed the comet-shaped plaques of HAdV-C2-dE3B-GFP, and yielded confined, predominantly round-shaped infection foci 4 dpi, akin to Nelfinavir-treated infections (Figure 5B).

To test if round-shaped infection foci (plaques) occurred in regular HAdV-C2-dE3B-GFP infections, we analysed A549 cells infected with less than one plaque forming unit (pfu) per well in 160 wells up to 8 dpi. Thirty three wells developed a single plaque. Twenty four of them were fast emerging comet-shaped plaques, of which the donor cell (indicated by the pink arrow), disappeared between 2 and 3 dpi (Figure 5C, upper panel). In contrast, nine wells developed delayed round plaques starting 6 dpi (Figure 5D, lower panel). In all these cases, the original infected cell (orange arrow) remained GFP-positive and apparently viable, and the surrounding cells gradually became infected. These data suggest that HAdV-C2 utilizes both lytic and non-lytic transmission, the former involving cell-free transmission, and the latter cell-associated transmission.

Nelfinavir has a broad anti-HAdV spectrum

We finally assessed the inhibition breadth of Nelfinavir against various HAdV types from species A, B, C and D in different human cell lines, as well as mouse adenovirus (MAdV) 1 and 3 in mouse rectum carcinoma CMT93 cells. To balance statistical significance and automated plaque segmentation, we first determined the optimal amount of inoculum and duration of infection for each virus and cell line. The resulting TI_{50} values of Nelfinavir were heterogeneous for different HAdV types, as determined in A549 cells (Figure 6A, for details see Supplementary Table 2). While all the tested HAdV-C types as well as HAdV-B14 showed high TI_{50}s (>10) ranging from 12.22 (HAdV-C1) to 71.09 (HAdV-C2). Members of HAdV species A, D and most of the HAdV-B types showed intermediate (2 - 10) to low Nelfinavir susceptibility (<2), notably HAdV-B7 and B11 with TI_{50}<1. MAdV-1 and 3 also showed low susceptibility. Noticeably, a high susceptibility of HAdV-C was consistently observed in human lung epithelial carcinoma (A549) cells, human epithelial cervix carcinoma (HeLa) cells, immortalized primary normal human corneal epithelial (HCE) cells as well as normal human bronchial epithelial (HBEC) cells. The corresponding TI_{50} values were in the same range as for herpes simplex virus (HSV) 1, for which Nelfinavir was reported to be an egress inhibitor (133, 138, 139).

We finally examined the plaque morphologies in non-perturbed infections by immunofluorescence staining of the late proteins VI and hexon, as well as macroscopic analyses of crystal violet stained dishes for classical plaques (Figure 6B). Viruses that were highly susceptible to Nelfinavir (exhibiting high TI_{50} values) formed exclusively comet-shaped plaques. Viruses with low TI_{50} values, such as A31, B11 or D37 had a high fraction of round plaques, even when infected with more than 1 pfu / well. This demonstrates that the slowly growing round infection foci observed in fluorescent microscopy gave similarly shaped lesions due to cytotoxicity, akin to the lytic comet-shaped foci. We conclude that HAdV types employ lytic cell-free and non-lytic cell-to-cell transmission modes and give rise to different plaque phenotypes.

Antimicrobial Agents and Chemotherapy
AAC
Antimicrobial Agents and Chemotherapy
Downloaded from http://aac.asm.org/ on July 13, 2020 by guest

Accepted Manuscript Posted Online

Discussion

A phenotypic screen of the PCL identified Nelfinavir as a potent, post-exposure inhibitor of HAdV-C2-dE3B-GFP plaque formation in cell culture (100). Nelfinavir is a non-nucleoside class inhibitor against a range of HAdV types. Surprisingly, we found Nelfinavir to inhibit HAdV infection, although Nelfinavir was previously classified as inactive against HAdV-C based on replication assays (133). It is the off-patent FDA-approved active pharmaceutical ingredient of Viracept. Nelfinavir was originally developed as an inhibitor against the HIV aspartyl protease. It is orally bioavailable, with an inhibitory concentration in the low nanomolar range (102, 132). Nelfinavir inhibits the replication of enveloped viruses, including SARS coronavirus (140), hepatitis C virus (141) as well as α-, β- and γ-herpes viruses (133). In the case of the α-herpes virus HSV-1, Nelfinavir inhibits the envelopment of the capsid with cytoplasmic membranes. This coincided with impaired glycosylation of gB and gC in the TGN (133, 138, 139, 142). Nelfinavir was reported to inhibit the activity of regulatory proteases in the Golgi, the growth of cancer cells and to induce a wealth of other effects, including autophagy, ER stress, the unfolded protein response, and apoptosis (143–149) (150–152, reviewed in 153–155). It remains unknown if Nelfinavir exerts these pleiotropic effects by interfering with diverse processes or a particular one.

Here, we demonstrate that Nelfinavir inhibits the egress of HAdV particles without perturbing other viral replication steps including entry, assembly and maturation. Morphometric analyses of the fluorescent plaques indicated that HAdV-C propagates by two distinct mechanisms, lytic and non-lytic. Lytic transmission led to comet-shaped convection driven plaques, whereas non-lytic transmission gave rise to symmetric round-shaped plaques. Nelfinavir specifically suppressed the lytic spread of HAdV, most prominently the HAdV-C types and B14, but not other HAdV, such as A31 or D37. Incidentally, HAdV-C and B14 replicate to considerable levels in Syrian hamsters, whereas other HAdV types do not (31, 156, 157). We infer that lytic infection could be a pathogenicity driver, at least in the hamster model.

The molecular mechanisms underlying cell lysis in AdV infection are not well understood, largely due to the lack of specific assays and inhibitors. Single cell analyses combined with machine learning start to identify specific features of lytic cells, such as increased intra-nuclear pressure compared to non-lytic cells (158). The lysis induced by HAdV was suggested to involve caspase-dependent functions, and necrosis-like features (99, 159, 160). The best characterized factor in HAdV cell lysis is ADP, a small membrane protein encoded in HAdV-C (90, 91, 161). ADP-deletion mutants show delayed onset of plaque formation (73, 135). Lysis is enhanced by increased ADP levels and tuned by post-translational ADP processing (73, 74, 135). ADP has a single signal/anchor sequence, and its lumenal domain is N- and O-glycosylated. The N-terminal segment is cleaved off in the Golgi lumen, and the membrane-anchored ADP localizes to the inner nuclear membrane (92, 107, 135). Interestingly, two cysteine residues in the cytoplasmic domain adjacent to the transmembrane segment are palmitoylated (107) (162). S-palmitoylation is known to support anchorage and sorting of host and viral membrane proteins.

Antimicrobial Agents and Chemotherapy
AAC
Antimicrobial Agents and Chemotherapy
Downloaded from http://aac.asm.org/ on July 13, 2020 by guest

Accepted Manuscript Posted Online

Accordingly, S-palmitoylation in the Golgi facilitates protein oligomerization, virion assembly and entry, as shown for structural proteins of enveloped viruses, including SARS-CoV-1 S, vesicular stomatitis virus G, sindbis virus E2, influenza virus HA, respiratory syncytial virus F, or rubella virus E1 and E2, as well as viroporin-mediated membrane permeabilization, including mouse hepatitis virus E protein, SARS-CoV-1 E protein and sindbis virus 6K. For reviews, see (163, 164).

Conspicuously, the cell lysis defective HAdV mutant pm734.4 encodes a C2 mutant ADP with two point mutations in the transmembrane domain, $C_{53}R$ and $M_{56}L$ (107). The mutant ADP localizes to the ER and the nuclear envelope, but not the Golgi, unlike the parental wild type virus rec700. The localization of the pm734.4 ADP is akin to the localization of HAdV-C2 ADP in Nelfinavir-treated cells, which resist lysis and lack ADP localization in the Golgi. We speculate that the palmitoylation of ADP in the Golgi is crucial for ADP to enhance the rupture of the nuclear membrane in lytic HAdV-C egress. Nelfinavir may interfere with ADP palmitoylation either by inhibiting a palmitoyl-acyltransferase or by dispersing the donor substrate for protein palmitoylation, palmitoyl-coenzyme A (164). Remarkably, Nelfinavir has a high logP value, 4.1 to 4.68 (165, 166), and partitions into lipophilic domains of the cell, including membranes. This is akin to another lipophilic drug with pleiotropic effects, the anti-viral and anti-helminthic compound Niclosamide, which is a weak acid and acts as a protonophore extracting protons from acidic organelles, and thereby inhibits virus entry and uncouples mitochondrial proton gradients (167, 168).

We noticed that ADP is not the sole lysis factor of HAdV. HAdV types lacking ADP, such as B types, also release their progeny by lysis, albeit with efficacies that vary depending on the cell type (169–171). This is in agreement with the observation that HAdV types of the A, B and D species form comet-shaped plaques, and that ADP-deleted HAdV-C2 lyse the host cell, and form comet-shaped plaques, albeit delayed and with lower efficacy than ADP-containing rec700 or HAdV-C2-dE3B-GFP. Conspicuously, other AdV proteins besides ADP were reported to interfere with cell lysis, such as the early region 4 ORF4 protein, which induces nuclear envelope blebbing and promotes the loss of nuclear integrity (172, 173). This, together with diverse cellular mechanisms underlying force generation and membrane rupture, could compensate for the lack of ADP in some forms of lytic virus egress (51, 55, 173). We consider it unlikely that genetic variability of the inoculum accounts for the presence of lytic and non-lytic pathways, since the inoculum was derived from an infectious DNA clone of HAdV-C2-dE3B-GFP, and lacked any mutations affecting amino acid coding across many passages (72).

In addition to providing a new inhibitor of lytic HAdV propagation, Nelfinavir revealed an alternative non-lytic HAdV transmission pathway, which gives rise to slow-growing symmetrical plaques. This non-lytic pathway exists in unperturbed cells, but is camouflaged by the rapid and far-reaching lytic infection. The non-lytic egress pathway is likely a deterministic process. It is stable for at least eight days (see Fig. 5C). It remains to be explored if cells can switch between the lytic and the non-lytic pathway. Regardless, non-lytic egress from the nucleus bypasses the nuclear envelope and the plasma membrane. We speculate that the non-lytic pathway involves

Antimicrobial Agents and Chemotherapy
AAC
Antimicrobial Agents and Chemotherapy
Downloaded from http://aac.asm.org/ on July 13, 2020 by guest

Accepted Manuscript Posted Online

sorting of HAdV particles to membrane sites where outward budding and scission occur. HAdV budding through the nuclear envelope could involve the WASH complex, akin to nuclear release of large RNPs in Drosophila, and perhaps similar to HSV budding (174, 175). Cytoplasmic membrane budding could be enhanced by the ESCRT complex, which is known to release enveloped viruses, such as HIV, and also facultative-enveloped viruses, such as hepatitis A virus (176–178). Alternatively, autophagy could sequester virions from the nucleus and upon fusion with the plasma membrane release virions from infected cell.

In conclusion, our work opens new therapeutic options for treating adenovirus disease, including acute and persistent infections. For example, HAdV-C persists in lymphocytes, which resist lytic infection, but also in epithelial cell lines under the repression of interferon and activation of the unfolded protein response sensor IRE-1a (122, 123, 179–182). Nelfinavir might be considered for anti-HAdV therapy, for example prophylactically in hematopoietic stem cell recipients, whose life is threatened by reactivation of HAdV-C (5, 6, 183).

Antimicrobial Agents and Chemotherapy

AAC

Downloaded from http://aac.asm.org/ on July 13, 2020 by guest

Antimicrobial Agents and Chemotherapy

Accepted Manuscript Posted Online

Contributions

UFG, VA and AY conceived the project. FG, VA, RW, LY, MG and NM performed experiments. FG, VA, RW, LM, FK, VP, AY, GT, UFG analysed data. SH contributed essential viruses. FG and UFG wrote the manuscript.

Acknowledgements

We thank Anja Ehrhardt for providing the HAdV-C-neutralizing dog serum. William SM Wold and Anne Tollefson kindly provided the α-ADP antibodies and ADP mutant viruses. Albert Heim provided HAdV-B14 and 21, Maarit Suomalainen provided HAdV-C2 and C5, discussions and advice. Yohei Yamauchi contributed Influenza A virus H1N1 virus and Cornel Fraefel the HSV-1-CMV-GFP. Vibhu Prasad kindly supported the impedance experiments. We are grateful for scientific discussions with Ivo Sbalzarini. We thank the Center for Microscopy and Image Analysis (ZMB) at UZH providing the EM instrumentation, and the members of the Greber lab for constructive discussions.

Conflict of interest

The authors declare no conflict of interest.

Funding

We acknowledge the financial support from the Swiss National Science Foundation (UFG, 31003A_179256 / 1), and the National Research Program “NCCR chemical biology” supported by the Swiss National Science Foundation (GT, UFG).

Abbreviations

ADP, adenovirus death protein;
AdV, adenovirus;
CAR, coxsackievirus adenovirus receptor;
CMV, cytomegalovirus;
DFT, 3′-Deoxy-3′-fluorothymidine;
DMEM, Dulbecco’s Modified Eagle medium;
dpi, day(s) post infection;
EC_{50}, 50% effective concentration;
GFP, green fluorescent protein;
HAdV, human adenovirus;
HIV, human immunodeficiency virus;
hpi, hour(s) post infection;
HSV, herpes simplex virus;
kbp, kilo base pairs,
MAdV, mouse adenovirus;
o/n, over night;
ORF, open reading frame;
Nelfinavir Mesylate, Nelfinavir;
pBI, pBluescript;
PCL, Prestwick Chemical Library;

Antimicrobial Agents and Chemotherapy
AAC
Antimicrobial Agents and Chemotherapy
Downloaded from http://aac.asm.org/ on July 13, 2020 by guest

Accepted Manuscript Posted Online

PFA, para-formaldehyde;
pfu, plaque forming unit(s);
pi, post infection;
PI, propidium iodide;
RT, room temperature;
SE, standard error;
SD, standard deviation;
TC_{50}, 50% toxic concentration;
TI, therapeutic index;
ts, temperature-sensitive;
VP, viral particles;
wt, wild type

Downloaded from http://aac.asm.org/ on July 13, 2020 by guest

Antimicrobial Agents and Chemotherapy
AAC
Antimicrobial Agents and Chemotherapy

Accepted Manuscript Posted Online

Figures

Figure 1: The small molecule Nelfinavir is a potent inhibitor of HAdV-C infection.

A Representative 384-well epifluorescence microscopy images of cells treated with DMSO (left), Nelfinavir (centre) and DFT (right), infected with HAdV-C2-dE3B-GFP for 72 h. Hoechst-stained nuclei are shown in blue, viral GFP in green. Dotted lines indicate well outline. Scale bar is 5 mm.
B Structural formula of Nelfinavir mesylate.
C The half-maximal toxicity (TC_{50}) in uninfected A549 cells was determined by Nelfinavir dose-response impedance measurements at different times of drug treatment. The x-axis indicates the time post cell seeding, as well as drug addition. Impedance was recorded at intervals of 15 min using xCELLigence reporting on the cell number and cell adhesion to the electrode-coated wells. The raw CI data are available in Supplementary Figure 1.
D Separation of effect (EC_{50}, plaque numbers) and toxicity (TC_{50}, nuclei numbers) of Nelfinavir in A549 cells at 82 hpi based on four technical replicates. Plaque numbers per well are depicted as red circles, and numbers of infected nuclei as green circles. Numbers of nuclei in Nelfinavir-treated, uninfected wells are shown in blue; treated, infected wells shown in orange.

Downloaded from http://aac.asm.org/ on July 13, 2020 by guest

Antimicrobial Agents and Chemotherapy
AAC
Antimicrobial Agents and Chemotherapy

Accepted Manuscript Posted Online

Figure 2. Nelfinavir does not affect early or late steps of HAdV-C infection.

A No effect of Nelfinavir on the expression of CMV-GFP (green) or the late viral protein hexon (red) in HAdV-C2-dE3B-GFP-infected A549 cells. Data points represent for each of the four biological replicates: mean median, nuclear intensities per well normalized to the mean median nuclear intensities of the DMSO-treated wells. Epifluorescence microscopy images were segmented and analysed using CellProfiler.

B Representative TEM images of late stage HAdV-C2-dE3B-GFP-infected A549 cells at 41 hpi reveal viral particles inside the nucleus in both DMSO-treated and Nelfinavir-treated cells (white arrow head). Black arrow heads indicate the nuclear envelope, arrow head with * points to rupture. Scale bar equivalent to 2 µm.

C Nelfinavir does not affect the maturation of HAdV-C5, as indicated by fully processed VI and VII proteins in purified particles grown in presence of Nelfinavir. Note that HAdV-C2-ts1 lacking the L3/p23 protease contains the precursor capsid proteins of VI and VII (pVI and pVII).

D HAdV-C5 grown in presence of Nelfinavir (HAdV-C5$^{+Nelfinavir}$) binds to naive A549 cells similar as HAdV-C5 from control cells. Cells were incubated with virus at 4°C for 1 h and fixed with PFA. Staining of viral capsids with an α-hexon antibody (green puncta). Nuclei shown with Hoechst staining (blue). Cells were visualized by NHS-ester staining (red). Images are max projections of confocal z stacks, and also show zoomed in views (grey squares). Scale bars = 20 µm.

E Particles produced in presence of Nelfinavir are fully infectious. A549 cells were inoculated with purified HAdV-C5 and incubated in absence (grey) or presence of Nelfinavir (orange colors) for 44 hpi. Infection analyses by α-hexon immunofluorescence staining, and cell numbers derived from Hoechst staining (blue). Bars represent means of four technical replicates. Error bars indicate standard deviation.

Antimicrobial Agents and Chemotherapy
AAC
Antimicrobial Agents and Chemotherapy
Downloaded from http://aac.asm.org/ on July 13, 2020 by guest

Accepted Manuscript Posted Online

Figure 3. Nelfinavir is a post-exposure inhibitor of HAdV-C egress.

A A549 cells were imaged at 3 days post inoculation with 1:10 diluted cell lysates (left) or supernatants (right) from Nelfinavir or control A549 cells, which had been infected with HAdV-C2-dE3B-GFP for the indicated times (harvested hpi). Results show delayed viral progeny release to the supernatant of Nelfinair-treated cells. Nuclei are shown in blue, infection marker in green (GFP).

B Released and cell-associated progeny from HAdV-C2-dE3B-GFP-infected A549 cells treated with Nelfinavir (orange) or DMSO (green), as determined by titration on A549 cells in a 12-well assay format. Lines indicate mean slopes, dotted lines standard error. Linear regression of three biological triplicates.

C Time-resolved emergence of plaques in HAdV-C2-dE3B-GFP-infected A549 cells treated with 1.25 µM Nelfinavir. Plaques in infected, non-treated wells are shown in green, Nelfinavir-treated wells in orange and nuclei in blue. Data points represent one of eight technical replicates. Coloured vertical lines indicate means and error bars the standard deviations.

D The inhibitory effect of Nelfinavir on HAdV-C2-dE3B-GFP spread is dependent on the amount input virus during initial infection. Number of infected, GFP-positive cells shown in green at 3 µM Nelfinavir relative to the mean infection of solvent-treated cells infected with the corresponding dosage. Total number of nuclei shown in blue, number of PI-positive dead cells in red. Note that the number of infected cells at 43 hpi is not affected by the Nelfinavir treatment. Data points represent means of four technical replicates. Dotted lines indicate standard deviation.

E Treatment of HAdV-C2-dE3B-GFP-infected A549 cells with 1.25 µM Nelfinavir suppresses comet-shaped plaques and reveals slow growing quasi-round plaques. Viral GFP expression levels are shown as 16-color LUT. Scale bar is 1 mm.

F Treatment with 1.25 µM Nelfinavir inhibits HAdV-C2-dE3B-GFP infection of A549 cells by slowing plaque formation. The numbers of infected cells and plaques per well of DMSO-treated wells are shown in green, those of Nelfinavir-treated wells in orange. Data points represent means of 24 technical replicates, including the well shown in the micrographs of panel **D**. Error bars indicate standard deviation. Statistical significance of drug versus non-treated cells was derived by the Kolmogorov-Smirnov test, p value < 0.0001 (****).

G The delayed HAdV-C2-dE3B-GFP plaques in presence of 1.25 µM Nelfinavir are significantly rounder than control plaques, as indicated by Kolmogorov-Smirnov test. Data points indicate plaque regions in the well centre harbouring a single peak region. Summary of 24 technical replicates including the well shown in the micrographs of panel **D**. Regions consisting of at least 5 infected cells (≥1,500 µm^2) were considered as a plaque. Plaque morphologies in control wells could not be quantified later than 3 dpi due to rapid virus dissemination. Plaques from DMSO-treated cells 3 dpi compared to Nelfinavir-treated ones 5 dpi: approximate p value < 0.0001 (****). DMSO-treated plaques 3 dpi vs. Nelfinavir-treated plaques 6 dpi: approximate p value < 0.0001 (****). Statistical significance by Kolmogorov-Smirnov test.

Antimicrobial Agents and Chemotherapy
AAC
Antimicrobial Agents and Chemotherapy
Downloaded from http://aac.asm.org/ on July 13, 2020 by guest

Accepted Manuscript Posted Online

Figure 4. ADP contributes to the inhibitory effect of Nelfinavir against HAdV-C.

A The deletion of ADP from HAdV-C2-dE3B-GFP delays plaque formation in A549 cells by one day, but does not change plaque shape. Cells were infected with $1.1*10^5$ VP / well. GFP is in green, hexon staining red, Hoechst signal of nuclei blue. Scale bar is 1 mm.

B The deletion of ADP from HAdV-C2-dE3B-GFP reduces the antiviral effects of Nelfinavir in A549, with EC_{50} = 5.82 compared to 0.22 µM for the parental virus. HAdV-C2-dE3B-GFP infection was quantified at 72 hpi, and 96 hpi for the ADP deletion mutant. Plaque numbers per well were normalized to the mean DMSO control and depicted as full green triangles for HAdV-C2-dE3B-GFP and empty red triangles for the ADP deletion mutant. Nuclei numbers of non-infected, treated wells were normalized to the mean DMSO control and depicted as full blue circles (72 h incubation), and empty blue circles (96 h). Data points represent means of four technical replicates. Error bars indicate standard deviation. EC_{50} values were derived from non-linear curve fitting. For detailed information and statistics, see Supplementary Table 2.

C The delay of dell death was calculated from the highest mean cell index (CI) and its half maximum for each treatment (mean of two technical replicates). HAdV-C2-dE3B-GFP data in green and dADP in red. For HAdV-C2-dE3B-GFP-infected A549 treated with 25 µM Nelfinavir, the measurement was aborted due to overgrowth causing cytotoxicity before the maximal cell index was reached. Treatment with 100 µM Nelfinavir was toxic.

D Therapeutic index (TI_{50}) derived from the ratio of Nelfinavir concentration causing 50% toxicity (TC_{50}) and the concentration leading to 50% reduction in plaque numbers per well (EC_{50}). Results from different cancer and primary cells are shown for HAdV-C2-dE3B-GFP and HAdV-C2-dE3B-dADP lacking ADP. For detailed information and statistics, see Supplementary Table 2.

E Representative high-magnification confocal images of HAdV-C2-dE3B-GFP-infected A549 cells 44 hpi showing the effect of Nelfinavir on ADP localization (left panel). ADP was stained by immunofluorescence with a rabbit α-HAdV-C2-ADP_{87-101} antibody (red). Cells were stained using NHS-ester (grey scale). White arrow heads highlight infected cells. Nuclei (blue), viral GFP (green). Images are max projections of 30 z planes with 0.5 µm z steps. Scale bar 10 µm. Relative units (RU) of total ADP expression (grey), localization to the nuclear rim (blue) and granularity (red) normalized to the mean values from DMSO control cells (right panel). The data set is comprised of 20 Nelfinavir-treated infected cells, and 23 control cells. Solid lines indicate median, dotted lines the 5-95% quantile. Kolmogorov-Smirnov indicated an ADP granularity p value of 0.0019 (**).

Antimicrobial Agents and Chemotherapy
AAC
Antimicrobial Agents and Chemotherapy
Downloaded from http://aac.asm.org/ on July 13, 2020 by guest

Accepted Manuscript Posted Online

Figure 5: Round plaque phenotypes in presence of neutralising anti-HAdV-C2 antibodies and in unperturbed HAdV-C2 infections.

A Schematic overview of pathogen transmission routes in cell cultures. Cell lysis kills the donor cell and releases progeny, while non-lytic egress preserves the infected donor cell. Convection in the media leads to long-distance, comet-shaped plaques, and cell-free virus transmission is susceptible to neutralizing antibodies. In contrast, direct cell-to-cell spread of virus gives rise to symmetric slow growing plaques, resistant to neutralizing antibodies. Non-infected cells are shown in grey and nuclei in blue. First round infected cells are shown in dark green, nuclei with a ruptured envelope in red. Second round infected cells are shown in light green. Grey arrow represents direction of convective flow. Axes indicate side or top-down views.

B Inhibition of cell-free HAdV-C2-dE3B-GFP transmission by an anti-HAdV-C2/5-neutralizing serum. Nuclei are shown in blue, viral GFP in green.

C Infection of A549 cells with limiting amounts of HAdV-C2-dE3B-GFP (<1 pfu/ well, 9-75 VP/ well) in 160 wells gives rise to 33 single plaques / well. Twenty-four wells contained GFP-positive comet-shaped plaques (upper panel), and nine developed delayed round plaques (lower panel). Dashed coloured squares indicate magnified regions of first-round infected cell below. Infected cell leading to comet-shaped plaque (upper panel, pink arrow) lyses at 3 dpi as indicated by loss of GFP signal. Infected cell giving rise to round plaque (lower panel, orange arrow) remains GFP-positive. Scale bar is 1 mm.

Antimicrobial Agents and Chemotherapy
AAC
Antimicrobial Agents and Chemotherapy
Downloaded from http://aac.asm.org/ on July 13, 2020 by guest

Accepted Manuscript Posted Online

Figure 6: Susceptibility of HAdV to Nelfinavir correlates with plaque shape.

A Therapeutic index (TI_{50}) calculated from the ratio of Nelfinavir concentration causing 50% toxicity (TC_{50}) and the concentration leading to 50% plaque reduction (EC_{50}). Different HAdVs, mouse adenoviruses (MAdV) and herpes simplex virus 1 (HSV-1) were tested in different cancer and primary cell lines. For detailed information and statistics, see Supplementary Table 2.

B Representative microscopic and macroscopic plaque morphologies of Nelfinavir-sensitive and insensitive HAdV types. Grey scale images show plaques based on epifluorescence microscopy of hexon immunostaining or GFP expression in A549 cells (96 well format). Scale bar is 1 mm. Coloured images show plaques visualized by crystal violet staining in A549 cells (12 well format). Scale bar is 5 mm.

Antimicrobial Agents and Chemotherapy

AAC

Antimicrobial Agents and Chemotherapy

Downloaded from http://aac.asm.org/ on July 13, 2020 by guest

Accepted Manuscript Posted Online

Antimicrobial Agents and Chemotherapy

AAC

Antimicrobial Agents and Chemotherapy

Downloaded from http://aac.asm.org/ on July 13, 2020 by guest

References

1. **Rowe WP**, **Huebner RJ**, **Gilmore LK**, **Parrott RH**, **Ward TG**. 1953. Isolation of a cytopathogenic agent from human adenoids undergoing spontaneous degeneration in tissue culture. Proc Soc Exp Biol Med **84**:570–573.
2. **Ismail AM**, **Zhou X**, **Dyer DW**, **Seto D**, **Rajaiya J**, **Chodosh J**. 2019. Genomic foundations of evolution and ocular pathogenesis in human adenovirus species D. FEBS Lett. **593**:3583–3608.
3. **Harrach B**, **Tarján ZL**, **Benkő M**. 2019. Adenoviruses across the animal kingdom: a walk in the zoo. FEBS Lett.
4. **Mei Y-F**, **Lindman K**, **Wadell G**. 2002. Human adenoviruses of subgenera B, C, and E with various tropisms differ in both binding to and replication in the epithelial A549 and 293 cells. Virology **295**:30–43.
5. **Lynch JP**, **Kajon AE**. 2016. Adenovirus: epidemiology, global spread of novel serotypes, and advances in treatment and prevention. Semin Respir Crit Care Med **37**:586–602.
6. **Lion T**. 2019. Adenovirus persistence, reactivation, and clinical management. FEBS Lett.
7. **Krilov LR**. 2005. Adenovirus infections in the immunocompromised host. Pediatr. Infect. Dis. J. **24**:555–556.
8. **Greber UF**, **Arnberg N**, **Wadell G**, **Benkő M**, **Kremer EJ**. 2013. Adenoviruses - from pathogens to therapeutics: a report on the 10th International Adenovirus Meeting. Cell Microbiol. **15**:16–23.
9. **Bailey ES**, **Fieldhouse JK**, **Choi JY**, **Gray GC**. 2018. A mini review of the zoonotic threat potential of influenza viruses, coronaviruses, adenoviruses, and enteroviruses. Front Public Health **6**:104.
10. **Hwang S-M**, **Park D-E**, **Yang Y-I**, **Park S-J**, **Lee H-K**, **Kim M-J**, **Chun B-C**. 2013. Outbreak of febrile respiratory illness caused by adenovirus at a South Korean military training facility: clinical and radiological characteristics of adenovirus pneumonia. Jpn J Infect Dis **66**:359–365.
11. **Potter RN**, **Cantrell JA**, **Mallak CT**, **Gaydos JC**. 2012. Adenovirus-associated deaths in US military during postvaccination period, 1999-2010. Emerging Infect. Dis. **18**:507–509.
12. **Erdman DD**, **Xu W**, **Gerber SI**, **Gray GC**, **Schnurr D**, **Kajon AE**, **Anderson LJ**. 2002. Molecular epidemiology of adenovirus type 7 in the United States, 1966-2000. Emerging Infect. Dis. **8**:269–277.
13. **State of New Jersey Department of Health**. 2019. Adenovirus. Communicable Disease Service - Adenovirus.
14. **Deal C**, **Pekosz A**, **Ketner G**. 2013. Prospects for oral replicating adenovirus-vectored vaccines. Vaccine **31**:3236–3243.
15. **Radin JM**, **Hawksworth AW**, **Blair PJ**, **Faix DJ**, **Raman R**, **Russell KL**, **Gray GC**. 2014. Dramatic decline of respiratory illness among US military recruits after the renewed use of adenovirus vaccines. Clin. Infect. Dis. **59**:962–968.
16. **Centers for Disease Control and Prevention (CDC)**. 2007. Acute respiratory disease associated with adenovirus serotype 14--four states, 2006-2007. MMWR Morb. Mortal. Wkly. Rep. **56**:1181–1184.
17. **Louie JK**, **Kajon AE**, **Holodniy M**, **Guardia-LaBar L**, **Lee B**, **Petru AM**, **Hacker JK**, **Schnurr DP**. 2008. Severe pneumonia due to adenovirus serotype 14: a new respiratory threat? Clin. Infect. Dis. **46**:421–425.
18. **Lam E**, **Ramke M**, **Warnecke G**, **Schrepfer S**, **Kopfnagel V**, **Dobner T**, **Heim A**. 2015. Effective apical infection of differentiated human bronchial epithelial cells and induction of proinflammatory chemokines by the highly pneumotropic human adenovirus type 14p1. PLoS One **10**:e0131201.
19. **O'Flanagan D**, **O'Donnell J**, **Domegan L**, **Fitzpatrick F**, **Connell J**, **Coughlan S**, **De Gascun C**, **Carr MJ**. 2011. First reported cases of human adenovirus serotype 14p1 infection, Ireland, October 2009 to July 2010. Euro Surveill. **16**.
20. **Carr MJ**, **Kajon AE**, **Lu X**, **Dunford L**, **O'Reilly P**, **Holder P**, **De Gascun CF**, **Coughlan S**,

Accepted Manuscript Posted Online

Connell J, **Erdman DD**, **Hall WW**. 2011. Deaths associated with human adenovirus-14p1 infections, Europe, 2009-2010. Emerging Infect. Dis. **17**:1402–1408.

21. **Benkő M**, **Harrach B**, **Kremer EJ**. 2014. Do nonhuman primate or bat adenoviruses pose a risk for human health? Future Microbiol **9**:269–272.

22. **Chen EC**, **Yagi S**, **Kelly KR**, **Mendoza SP**, **Tarara RP**, **Canfield DR**, **Maninger N**, **Rosenthal A**, **Spinner A**, **Bales KL**, **Schnurr DP**, **Lerche NW**, **Chiu CY**. 2011. Cross-species transmission of a novel adenovirus associated with a fulminant pneumonia outbreak in a new world monkey colony. PLoS Pathog. **7**:e1002155.

23. **To KKW**, **Tse H**, **Chan W-M**, **Choi GKY**, **Zhang AJX**, **Sridhar S**, **Wong SCY**, **Chan JFW**, **Chan ASF**, **Woo PCY**, **Lau SKP**, **Lo JYC**, **Chan K-H**, **Cheng VCC**, **Yuen K-Y**. 2014. A novel psittacine adenovirus identified during an outbreak of avian chlamydiosis and human psittacosis: zoonosis associated with virus-bacterium coinfection in birds. PLoS Negl. Trop. Dis. **8**:e3318.

24. **Gray GC**, **McCarthy T**, **Lebeck MG**, **Schnurr DP**, **Russell KL**, **Kajon AE**, **Landry ML**, **Leland DS**, **Storch GA**, **Ginocchio CC**, **Robinson CC**, **Demmler GJ**, **Saubolle MA**, **Kehl SC**, **Selvarangan R**, **Miller MB**, **Chappell JD**, **Zerr DM**, **Kiska DL**, **Halstead DC**, **Capuano AW**, **Setterquist SF**, **Chorazy ML**, **Dawson JD**, **Erdman DD**. 2007. Genotype prevalence and risk factors for severe clinical adenovirus infection, United States 2004-2006. Clin. Infect. Dis. **45**:1120–1131.

25. **Metzgar D**, **Osuna M**, **Kajon AE**, **Hawksworth AW**, **Irvine M**, **Russell KL**. 2007. Abrupt emergence of diverse species B adenoviruses at US military recruit training centers. J. Infect. Dis. **196**:1465–1473.

26. **Haque E**, **Banik U**, **Monowar T**, **Anthony L**, **Adhikary AK**. 2018. Worldwide increased prevalence of human adenovirus type 3 (HAdV-3) respiratory infections is well correlated with heterogeneous hypervariable regions (HVRs) of hexon. PLoS One **13**:e0194516.

27. **Ginn SL**, **Amaya AK**, **Alexander IE**, **Edelstein M**, **Abedi MR**. 2018. Gene therapy clinical trials worldwide to 2017: An update. J Gene Med **20**:e3015.

28. **Jiang H**, **Gomez-Manzano C**, **Rivera-Molina Y**, **Lang FF**, **Conrad CA**, **Fueyo J**. 2015. Oncolytic adenovirus research evolution: from cell-cycle checkpoints to immune checkpoints. Curr Opin Virol **13**:33–39.

29. **Lawler SE**, **Speranza M-C**, **Cho C-F**, **Chiocca EA**. 2017. Oncolytic viruses in cancer treatment: A review. JAMA Oncol. **3**:841–849.

30. **Hiwarkar P**, **Amrolia P**, **Sivaprakasam P**, **Lum SH**, **Doss H**, **O'Rafferty C**, **Petterson T**, **Patrick K**, **Silva J**, **Slatter M**, **Lawson S**, **Rao K**, **Steward C**, **Gassas A**, **Veys P**, **Wynn R**, **United Kingdom Paediatric Bone Marrow Transplant Group**. 2017. Brincidofovir is highly efficacious in controlling adenoviremia in pediatric recipients of hematopoietic cell transplant. Blood **129**:2033–2037.

31. **Wold WSM**, **Tollefson AE**, **Ying B**, **Spencer JF**, **Toth K**. 2019. Drug development against human adenoviruses and its advancement by Syrian hamster models. FEMS Microbiol. Rev. **43**:380–388.

32. **Reddy VS**, **Natchiar SK**, **Stewart PL**, **Nemerow GR**. 2010. Crystal structure of human adenovirus at 3.5 A resolution. Science **329**:1071–1075.

33. **Benevento M**, **Di Palma S**, **Snijder J**, **Moyer CL**, **Reddy VS**, **Nemerow GR**, **Heck AJR**. 2014. Adenovirus composition, proteolysis, and disassembly studied by in-depth qualitative and quantitative proteomics. J. Biol. Chem. **289**:11421–11430.

34. **Flatt JW**, **Greber UF**. 2017. Viral mechanisms for docking and delivering at nuclear pore complexes. Semin. Cell Dev. Biol. **68**:59–71.

35. **Liu H**, **Jin L**, **Koh SBS**, **Atanasov I**, **Schein S**, **Wu L**, **Zhou ZH**. 2010. Atomic structure of human adenovirus by cryo-EM reveals interactions among protein networks. Science **329**:1038–1043.

36. **Greber UF**, **Flatt JW**. 2019. Adenovirus entry: from infection to immunity. Annu. Rev. Virol. **6**:177–197.

37. **Wang I-H**, **Burckhardt CJ**, **Yakimovich A**, **Greber UF**. 2018. Imaging, Tracking and

Antimicrobial Agents and Chemotherapy
AAC
Antimicrobial Agents and Chemotherapy
Downloaded from http://aac.asm.org/ on July 13, 2020 by guest

Accepted Manuscript Posted Online

Computational Analyses of Virus Entry and Egress with the Cytoskeleton. Viruses **10**.

38. **Suomalainen M**, **Greber UF**. 2013. Uncoating of non-enveloped viruses. Curr Opin Virol **3**:27–33.
39. **Greber UF**. 2002. Signalling in viral entry. Cellular and Molecular Life Sciences (CMLS) **59**:608–626.
40. **Sohn S-Y**, **Hearing P**. 2019. Adenoviral strategies to overcome innate cellular responses to infection. FEBS Lett. **593**:3484–3495.
41. **Prusinkiewicz MA**, **Mymryk JS**. 2019. Metabolic reprogramming of the host cell by human adenovirus infection. Viruses **11**.
42. **Pied N**, **Wodrich H**. 2019. Imaging the adenovirus infection cycle. FEBS Lett. **593**:3419–3448.
43. **Oliveira ERA**, **Bouvier M**. 2019. Immune evasion by adenoviruses: a window into host-virus adaptation. FEBS Lett. **593**:3496–3503.
44. **Nemerow G**, **Flint J**. 2019. Lessons learned from adenovirus (1970-2019). FEBS Lett. **593**:3395–3418.
45. **Lynch KL**, **Gooding LR**, **Garnett-Benson C**, **Ornelles DA**, **Avgousti DC**. 2019. Epigenetics and the dynamics of chromatin during adenovirus infections. FEBS Lett. **593**:3551–3570.
46. **Kleinberger T**. 2019. Biology of the adenovirus E4orf4 protein: from virus infection to cancer cell death. FEBS Lett.
47. **Hidalgo P**, **Ip WH**, **Dobner T**, **Gonzalez RA**. 2019. The biology of the adenovirus E1B 55K protein. FEBS Lett. **593**:3504–3517.
48. **Charman M**, **Herrmann C**, **Weitzman MD**. 2019. Viral and cellular interactions during adenovirus DNA replication. FEBS Lett. **593**:3531–3550.
49. **Atasheva S**, **Yao J**, **Shayakhmetov DM**. 2019. Innate immunity to adenovirus: lessons from mice. FEBS Lett. **593**:3461–3483.
50. **Allen RJ**, **Byrnes AP**. 2019. Interaction of adenovirus with antibodies, complement, and coagulation factors. FEBS Lett. **593**:3449–3460.
51. **Burckhardt CJ**, **Suomalainen M**, **Schoenenberger P**, **Boucke K**, **Hemmi S**, **Greber UF**. 2011. Drifting motions of the adenovirus receptor CAR and immobile integrins initiate virus uncoating and membrane lytic protein exposure. Cell Host Microbe **10**:105–117.
52. **Meier O**, **Greber UF**. 2004. Adenovirus endocytosis. J Gene Med **6 Suppl 1**:S152-63.
53. **Gastaldelli M**, **Imelli N**, **Boucke K**, **Amstutz B**, **Meier O**, **Greber UF**. 2008. Infectious adenovirus type 2 transport through early but not late endosomes. Traffic **9**:2265–2278.
54. **Wolfrum N**, **Greber UF**. 2013. Adenovirus signalling in entry. Cell Microbiol. **15**:53–62.
55. **Luisoni S**, **Suomalainen M**, **Boucke K**, **Tanner LB**, **Wenk MR**, **Guan XL**, **Grzybek M**, **Coskun Ü**, **Greber UF**. 2015. Co-option of Membrane Wounding Enables Virus Penetration into Cells. Cell Host Microbe **18**:75–85.
56. **Wiethoff CM**, **Wodrich H**, **Gerace L**, **Nemerow GR**. 2005. Adenovirus protein VI mediates membrane disruption following capsid disassembly. J. Virol. **79**:1992–2000.
57. **Leopold PL**, **Kreitzer G**, **Miyazawa N**, **Rempel S**, **Pfister KK**, **Rodriguez-Boulan E**, **Crystal RG**. 2000. Dynein- and microtubule-mediated translocation of adenovirus serotype 5 occurs after endosomal lysis. Hum. Gene Ther. **11**:151–165.
58. **Suomalainen M**, **Nakano MY**, **Keller S**, **Boucke K**, **Stidwill RP**, **Greber UF**. 1999. Microtubule-dependent plus- and minus end-directed motilities are competing processes for nuclear targeting of adenovirus. J. Cell Biol. **144**:657–672.
59. **Wang I-H**, **Burckhardt CJ**, **Yakimovich A**, **Morf MK**, **Greber UF**. 2017. The nuclear export factor CRM1 controls juxta-nuclear microtubule-dependent virus transport. J. Cell Sci. **130**:2185–2195.
60. **Zhou J**, **Scherer J**, **Yi J**, **Vallee RB**. 2018. Role of kinesins in directed adenovirus transport and cytoplasmic exploration. PLoS Pathog. **14**:e1007055.
61. **Bremner KH**, **Scherer J**, **Yi J**, **Vershinin M**, **Gross SP**, **Vallee RB**. 2009. Adenovirus transport via direct interaction of cytoplasmic dynein with the viral capsid hexon subunit. Cell Host Microbe

Antimicrobial Agents and Chemotherapy
AAC
Antimicrobial Agents and Chemotherapy
Downloaded from http://aac.asm.org/ on July 13, 2020 by guest

Accepted Manuscript Posted Online

6:523–535.

62. **Bauer M**, **Flatt JW**, **Seiler D**, **Cardel B**, **Emmenlauer M**, **Boucke K**, **Suomalainen M**, **Hemmi S**, **Greber UF**. 2019. The e3 ubiquitin ligase mind bomb 1 controls adenovirus genome release at the nuclear pore complex. Cell Rep. **29**:3785–3795.e8.

63. **Pelka P**, **Ablack JNG**, **Fonseca GJ**, **Yousef AF**, **Mymryk JS**. 2008. Intrinsic structural disorder in adenovirus E1A: a viral molecular hub linking multiple diverse processes. J. Virol. **82**:7252–7263.

64. **King CR**, **Zhang A**, **Tessier TM**, **Gameiro SF**, **Mymryk JS**. 2018. Hacking the cell: network intrusion and exploitation by adenovirus E1A. MBio **9**.

65. **Berk AJ**. 2005. Recent lessons in gene expression, cell cycle control, and cell biology from adenovirus. Oncogene **24**:7673–7685.

66. **Ferrari R**, **Pellegrini M**, **Horwitz GA**, **Xie W**, **Berk AJ**, **Kurdistani SK**. 2008. Epigenetic reprogramming by adenovirus e1a. Science **321**:1086–1088.

67. **Rao L**, **Debbas M**, **Sabbatini P**, **Hockenbery D**, **Korsmeyer S**, **White E**. 1992. The adenovirus E1A proteins induce apoptosis, which is inhibited by the E1B 19-kDa and Bcl-2 proteins. Proc. Natl. Acad. Sci. USA **89**:7742–7746.

68. **Zemke NR**, **Berk AJ**. 2017. The adenovirus E1A C terminus suppresses a delayed antiviral response and modulates RAS signaling. Cell Host Microbe **22**:789–800.e5.

69. **Greber UF**. 1998. Virus assembly and disassembly: the adenovirus cysteine protease as a trigger factor. Rev Med Virol **8**:213–222.

70. **Mangel WF**, **San Martín C**. 2014. Structure, function and dynamics in adenovirus maturation. Viruses **6**:4536–4570.

71. **Ahi YS**, **Mittal SK**. 2016. Components of adenovirus genome packaging. Front. Microbiol. **7**:1503.

72. **Yakimovich A**, **Gumpert H**, **Burckhardt CJ**, **Lütschg VA**, **Jurgeit A**, **Sbalzarini IF**, **Greber UF**. 2012. Cell-free transmission of human adenovirus by passive mass transfer in cell culture simulated in a computer model. J. Virol. **86**:10123–10137.

73. **Tollefson AE**, **Scaria A**, **Hermiston TW**, **Ryerse JS**, **Wold LJ**, **Wold WS**. 1996. The adenovirus death protein (E3-11.6K) is required at very late stages of infection for efficient cell lysis and release of adenovirus from infected cells. J. Virol. **70**:2296–2306.

74. **Doronin K**, **Toth K**, **Kuppuswamy M**, **Krajcsi P**, **Tollefson AE**, **Wold WSM**. 2003. Overexpression of the ADP (E3-11.6K) protein increases cell lysis and spread of adenovirus. Virology **305**:378–387.

75. **Haisma HJ**, **Kamps JAAM**, **Kamps GK**, **Plantinga JA**, **Rots MG**, **Bellu AR**. 2008. Polyinosinic acid enhances delivery of adenovirus vectors in vivo by preventing sequestration in liver macrophages. J. Gen. Virol. **89**:1097–1105.

76. **Kajon AE**, **Gigliotti AP**, **Harrod KS**. 2003. Acute inflammatory response and remodeling of airway epithelium after subspecies B1 human adenovirus infection of the mouse lower respiratory tract. J. Med. Virol. **71**:233–244.

77. **Beerli C**, **Yakimovich A**, **Kilcher S**, **Reynoso GV**, **Fläschner G**, **Müller DJ**, **Hickman HD**, **Mercer J**. 2019. Vaccinia virus hijacks EGFR signalling to enhance virus spread through rapid and directed infected cell motility. Nat. Microbiol. **4**:216–225.

78. **Roberts KL**, **Smith GL**. 2008. Vaccinia virus morphogenesis and dissemination. Trends Microbiol. **16**:472–479.

79. **Doceul V**, **Hollinshead M**, **van der Linden L**, **Smith GL**. 2010. Repulsion of superinfecting virions: a mechanism for rapid virus spread. Science **327**:873–876.

80. **Zhong P**, **Agosto LM**, **Munro JB**, **Mothes W**. 2013. Cell-to-cell transmission of viruses. Curr Opin Virol **3**:44–50.

81. **Mothes W**, **Sherer NM**, **Jin J**, **Zhong P**. 2010. Virus cell-to-cell transmission. J. Virol. **84**:8360–8368.

Antimicrobial Agents and Chemotherapy

AAC

Antimicrobial Agents and Chemotherapy

Downloaded from http://aac.asm.org/ on July 13, 2020 by guest

Accepted Manuscript Posted Online

82. **Burckhardt CJ**, **Greber UF**. 2009. Virus movements on the plasma membrane support infection and transmission between cells. PLoS Pathog. **5**:e1000621.

83. **van der Grein SG**, **Defourny KAY**, **Slot EFJ**, **Nolte-'t Hoen ENM**. 2018. Intricate relationships between naked viruses and extracellular vesicles in the crosstalk between pathogen and host. Semin Immunopathol **40**:491–504.

84. **Jansens RJJ**, **Tishchenko A**, **Favoreel HW**. 2020. Bridging the Gap: Virus Long-Distance Spread via Tunneling Nanotubes. J. Virol. **94**.

85. **Danthi P**. 2016. Viruses and the diversity of cell death. Annu. Rev. Virol. **3**:533–553.

86. **Madan V**, **Castelló A**, **Carrasco L**. 2008. Viroporins from RNA viruses induce caspase-dependent apoptosis. Cell Microbiol. **10**:437–451.

87. **Scott C**, **Griffin S**. 2015. Viroporins: structure, function and potential as antiviral targets. J. Gen. Virol. **96**:2000–2027.

88. **Zhang Y**, **Chen X**, **Gueydan C**, **Han J**. 2018. Plasma membrane changes during programmed cell deaths. Cell Res. **28**:9–21.

89. **Dhingra A**, **Hage E**, **Ganzenmueller T**, **Böttcher S**, **Hofmann J**, **Hamprecht K**, **Obermeier P**, **Rath B**, **Hausmann F**, **Dobner T**, **Heim A**. 2019. Molecular evolution of human adenovirus (hadv) species C. Sci. Rep. **9**:1039.

90. **Robinson CM**, **Singh G**, **Lee JY**, **Dehghan S**, **Rajaiya J**, **Liu EB**, **Yousuf MA**, **Betensky RA**, **Jones MS**, **Dyer DW**, **Seto D**, **Chodosh J**. 2013. Molecular evolution of human adenoviruses. Sci. Rep. **3**:1812.

91. **Davison AJ**, **Akter P**, **Cunningham C**, **Dolan A**, **Addison C**, **Dargan DJ**, **Hassan-Walker AF**, **Emery VC**, **Griffiths PD**, **Wilkinson GWG**. 2003. Homology between the human cytomegalovirus RL11 gene family and human adenovirus E3 genes. J. Gen. Virol. **84**:657–663.

92. **Scaria A**, **Tollefson AE**, **Saha SK**, **Wold WS**. 1992. The E3-11.6K protein of adenovirus is an Asn-glycosylated integral membrane protein that localizes to the nuclear membrane. Virology **191**:743–753.

93. **Georgi F**, **Greber UF**. 2020. The Adenovirus Death Protein - A small membrane protein controls cell lysis and disease. FEBS Lett. DOI: 10.1002/1873-3468.13848

94. **Tollefson AE**, **Scaria A**, **Saha SK**, **Wold WS**. 1992. The 11,600-MW protein encoded by region E3 of adenovirus is expressed early but is greatly amplified at late stages of infection. J. Virol. **66**:3633–3642.

95. **Wold WS**, **Cladaras C**, **Magie SC**, **Yacoub N**. 1984. Mapping a new gene that encodes an 11,600-molecular-weight protein in the E3 transcription unit of adenovirus 2. J. Virol. **52**:307–313.

96. **Ito H**, **Aoki H**, **Kühnel F**, **Kondo Y**, **Kubicka S**, **Wirth T**, **Iwado E**, **Iwamaru A**, **Fujiwara K**, **Hess KR**, **Lang FF**, **Sawaya R**, **Kondo S**. 2006. Autophagic cell death of malignant glioma cells induced by a conditionally replicating adenovirus. J. Natl. Cancer Inst. **98**:625–636.

97. **Jiang H**, **Gomez-Manzano C**, **Aoki H**, **Alonso MM**, **Kondo S**, **McCormick F**, **Xu J**, **Kondo Y**, **Bekele BN**, **Colman H**, **Lang FF**, **Fueyo J**. 2007. Examination of the therapeutic potential of Delta-24-RGD in brain tumor stem cells: role of autophagic cell death. J. Natl. Cancer Inst. **99**:1410–1414.

98. **Jiang H**, **White EJ**, **Ríos-Vicil CI**, **Xu J**, **Gomez-Manzano C**, **Fueyo J**. 2011. Human adenovirus type 5 induces cell lysis through autophagy and autophagy-triggered caspase activity. J. Virol. **85**:4720–4729.

99. **Abou El Hassan MAI**, **van der Meulen-Muileman I**, **Abbas S**, **Kruyt FAE**. 2004. Conditionally replicating adenoviruses kill tumor cells via a basic apoptotic machinery-independent mechanism that resembles necrosis-like programmed cell death. J. Virol. **78**:12243–12251.

100. **Georgi F**, **Kuttler F**, **Murer L**, **Andriasyan V**, **Witte R**, **Yakimovich A**, **Turcatti G**, **Greber UF**. 2020. High-content image-based drug screen identifies a clinical compound against cell transmission of adenovirus. BioRxiv. DOI: https://doi.org/10.1101/2020.05.15.098061

101. **Yakimovich A**, **Andriasyan V**, **Witte R**, **Wang I-H**, **Prasad V**, **Suomalainen M**, **Greber UF**. 2015. Plaque2.0-A High-Throughput Analysis Framework to Score Virus-Cell Transmission and

Antimicrobial Agents and Chemotherapy
AAC
Antimicrobial Agents and Chemotherapy
Downloaded from http://aac.asm.org/ on July 13, 2020 by guest

Accepted Manuscript Posted Online

Clonal Cell Expansion. PLoS One **10**:e0138760.

102. **Kaldor SW**, **Kalish VJ**, **Davies JF**, **Shetty BV**, **Fritz JE**, **Appelt K**, **Burgess JA**, **Campanale KM**, **Chirgadze NY**, **Clawson DK**, **Dressman BA**, **Hatch SD**, **Khalil DA**, **Kosa MB**, **Lubbehusen PP**, **Muesing MA**, **Patick AK**, **Reich SH**, **Su KS**, **Tatlock JH**. 1997. Viracept (nelfinavir mesylate, AG1343): a potent, orally bioavailable inhibitor of HIV-1 protease. J. Med. Chem. **40**:3979–3985.

103. **Greber UF**, **Willetts M**, **Webster P**, **Helenius A**. 1993. Stepwise dismantling of adenovirus 2 during entry into cells. Cell **75**:477–486.

104. **Warming S**, **Costantino N**, **Court DL**, **Jenkins NA**, **Copeland NG**. 2005. Simple and highly efficient BAC recombineering using galK selection. Nucleic Acids Res. **33**:e36.

105. **Sirena D**, **Lilienfeld B**, **Eisenhut M**, **Kälin S**, **Boucke K**, **Beerli RR**, **Vogt L**, **Ruedl C**, **Bachmann MF**, **Greber UF**, **Hemmi S**. 2004. The human membrane cofactor CD46 is a receptor for species B adenovirus serotype 3. J. Virol. **78**:4454–4462.

106. **Hemmi S**, **Geertsen R**, **Mezzacasa A**, **Peter I**, **Dummer R**. 1998. The presence of human coxsackievirus and adenovirus receptor is associated with efficient adenovirus-mediated transgene expression in human melanoma cell cultures. Hum. Gene Ther. **9**:2363–2373.

107. **Tollefson AE**, **Scaria A**, **Ying B**, **Wold WSM**. 2003. Mutations within the ADP (E3-11.6K) protein alter processing and localization of ADP and the kinetics of cell lysis of adenovirus-infected cells. J. Virol. **77**:7764–7778.

108. **Adrian T**, **Wadell G**, **Hierholzer JC**, **Wigand R**. 1986. DNA restriction analysis of adenovirus prototypes 1 to 41. Arch. Virol. **91**:277–290.

109. **Pacesa M**, **Hendrickx R**, **Bieri M**, **Flatt JW**, **Greber UF**, **Hemmi S**. 2017. Small-size recombinant adenoviral hexon protein fragments for the production of virus-type specific antibodies. Virol. J. **14**:158.

110. **Kajon AE**, **Hang J**, **Hawksworth A**, **Metzgar D**, **Hage E**, **Hansen CJ**, **Kuschner RA**, **Blair P**, **Russell KL**, **Jarman RG**. 2015. Molecular Epidemiology of Adenovirus Type 21 Respiratory Strains Isolated From US Military Trainees (1996-2014). J. Infect. Dis. **212**:871–880.

111. **Robinson M**, **Li B**, **Ge Y**, **Ko D**, **Yendluri S**, **Harding T**, **VanRoey M**, **Spindler KR**, **Jooss K**. 2009. Novel immunocompetent murine tumor model for evaluation of conditionally replication-competent (oncolytic) murine adenoviral vectors. J. Virol. **83**:3450–3462.

112. **Studer L**. 2017. Overcome the species barrier of productive human adenovirus infection in murine cells. Master thesis, Department of Molecular Life Sciences, University of Zurich.

113. **Jetzer T**. 2018. Characterization of the human/mouse adenovirus productive replication barrier by transcriptionally targeting genes of type B and C adenoviruses. Master thesis, Department of Molecular Life Sciences, University of Zurich.

114. **Wold WSM**, **Deutscher SL**, **Takemori N**, **Bhat BM**, **Magie SC**. 1986. Evidence that AGAUA and CCAGA initiate translation in the same mRNA in region E3 of adenovirus. Virology **148**:168–180.

115. **Bhat BM**, **Wold WS**. 1986. Adenovirus mutants with splice-enhancing mutations in the E3 complex transcription unit are also defective in E3A RNA 3'-end formation. J. Virol. **57**:1155–1158.

116. **Wold WS**, **Gooding LR**. 1991. Region E3 of adenovirus: a cassette of genes involved in host immunosurveillance and virus-cell interactions. Virology **184**:1–8.

117. **Hendrickx RC**. 2016. Study on Mouse Adenovirus Biology and Development of Their Vectors. Doctoral dissertation, Department of Molecular Life Sciences, University of Zurich.

118. **Bieri M**. 2018. Development of Adenovirus Reporter Viruses and Studies on Mouse Adenovirus-2 and -3 Receptor Candidates. Doctoral dissertation, Department of Molecular Life Sciences, University of Zurich.

119. **Glauser DL**, **Seyffert M**, **Strasser R**, **Franchini M**, **Laimbacher AS**, **Dresch C**, **de Oliveira AP**, **Vogel R**, **Büning H**, **Salvetti A**, **Ackermann M**, **Fraefel C**. 2010. Inhibition of herpes simplex virus type 1 replication by adeno-associated virus rep proteins depends on their combined DNA-binding and ATPase/helicase activities. J. Virol. **84**:3808–3824.

Antimicrobial Agents and Chemotherapy

AAC

Antimicrobial Agents and Chemotherapy

Downloaded from http://aac.asm.org/ on July 13, 2020 by guest

Accepted Manuscript Posted Online

120. **Ali A**, **Roossinck MJ**. 2007. Rapid and efficient purification of Cowpea chlorotic mottle virus by sucrose cushion ultracentrifugation. J. Virol. Methods **141**:84–86.

121. **Crameri M**, **Bauer M**, **Caduff N**, **Walker R**, **Steiner F**, **Franzoso FD**, **Gujer C**, **Boucke K**, **Kucera T**, **Zbinden A**, **Münz C**, **Fraefel C**, **Greber UF**, **Pavlovic J**. 2018. MxB is an interferon-induced restriction factor of human herpesviruses. Nat. Commun. **9**:1980.

122. **Prasad V**, **Suomalainen M**, **Pennauer M**, **Yakimovich A**, **Andriasyan V**, **Hemmi S**, **Greber UF**. 2014. Chemical induction of unfolded protein response enhances cancer cell killing through lytic virus infection. J. Virol. **88**:13086–13098.

123. **Prasad V**, **Suomalainen M**, **Jasiqi Y**, **Hemmi S**, **Hearing P**, **Hosie L**, **Burgert H-G**, **Greber UF**. 2020. The UPR sensor IRE1α and the adenovirus E3-19K glycoprotein sustain persistent and lytic infections. Nat. Commun. **11**:1997.

124. **Spiegel M**. 2009. Real-time and Dynamic Monitoring of Virus-mediated Cytopathogenicity. Biochemica 15–17.

125. **Carpenter AE**, **Jones TR**, **Lamprecht MR**, **Clarke C**, **Kang IH**, **Friman O**, **Guertin DA**, **Chang JH**, **Lindquist RA**, **Moffat J**, **Golland P**, **Sabatini DM**. 2006. CellProfiler: image analysis software for identifying and quantifying cell phenotypes. Genome Biol. **7**:R100.

126. **R Core Team**. 2018. R:A Language and Environment for Statistical Computing. Computer software, R Foundation for Statistical Computing, Vienna, Austria.

127. **Greber UF**, **Suomalainen M**, **Stidwill RP**, **Boucke K**, **Ebersold MW**, **Helenius A**. 1997. The role of the nuclear pore complex in adenovirus DNA entry. EMBO J. **16**:5998–6007.

128. **Baum SG**, **Horwitz MS**, **Maizel JV**. 1972. Studies of the mechanism of enhancement of human adenovirus infection in monkey cells by simian virus 40. J. Virol. **10**:211–219.

129. **Varghese R**, **Mikyas Y**, **Stewart PL**, **Ralston R**. 2004. Postentry neutralization of adenovirus type 5 by an antihexon antibody. J. Virol. **78**:12320–12332.

130. **Hausl MA**, **Zhang W**, **Müther N**, **Rauschhuber C**, **Franck HG**, **Merricks EP**, **Nichols TC**, **Kay MA**, **Ehrhardt A**. 2010. Hyperactive sleeping beauty transposase enables persistent phenotypic correction in mice and a canine model for hemophilia B. Mol. Ther. **18**:1896–1906.

131. **Topal MD**. 1984. Molecular mechanisms of chemical mutagenesis: 9-aminoacridine inhibits DNA replication in vitro by destabilizing the DNA growing point and interacting with the DNA polymerase. Biochemistry **23**:2367–2372.

132. **Moyle GJ**, **Youle M**, **Higgs C**, **Monaghan J**, **Prince W**, **Chapman S**, **Clendeninn N**, **Nelson MR**. 1998. Safety, pharmacokinetics, and antiretroviral activity of the potent, specific human immunodeficiency virus protease inhibitor nelfinavir: results of a phase I/II trial and extended follow-up in patients infected with human immunodeficiency virus. J. Clin. Pharmacol. **38**:736–743.

133. **Gantt S**, **Carlsson J**, **Ikoma M**, **Gachelet E**, **Gray M**, **Geballe AP**, **Corey L**, **Casper C**, **Lagunoff M**, **Vieira J**. 2011. The HIV protease inhibitor nelfinavir inhibits Kaposi's sarcoma-associated herpesvirus replication in vitro. Antimicrob. Agents Chemother. **55**:2696–2703.

134. **Imelli N**, **Ruzsics Z**, **Puntener D**, **Gastaldelli M**, **Greber UF**. 2009. Genetic reconstitution of the human adenovirus type 2 temperature-sensitive 1 mutant defective in endosomal escape. Virol. J. **6**:174.

135. **Tollefson AE**, **Ryerse JS**, **Scaria A**, **Hermiston TW**, **Wold WS**. 1996. The E3-11.6-kDa adenovirus death protein (ADP) is required for efficient cell death: characterization of cells infected with adp mutants. Virology **220**:152–162.

136. **Deutscher SL**, **Bhat BM**, **Pursley MH**, **Cladaras C**, **Wold WS**. 1985. Novel deletion mutants that enhance a distant upstream 5' splice in the E3 transcription unit of adenovirus 2. Nucleic Acids Res. **13**:5771–5788.

137. **Reily C**, **Stewart TJ**, **Renfrow MB**, **Novak J**. 2019. Glycosylation in health and disease. Nat. Rev. Nephrol. **15**:346–366.

138. **Kalu NN**, **Desai PJ**, **Shirley CM**, **Gibson W**, **Dennis PA**, **Ambinder RF**. 2014. Nelfinavir inhibits maturation and export of herpes simplex virus 1. J. Virol. **88**:5455–5461.

Antimicrobial Agents and Chemotherapy
AAC
Antimicrobial Agents and Chemotherapy
Downloaded from http://aac.asm.org/ on July 13, 2020 by guest

Accepted Manuscript Posted Online

139. **Gantt S**, **Gachelet E**, **Carlsson J**, **Barcy S**, **Casper C**, **Lagunoff M**. 2015. Nelfinavir impairs glycosylation of herpes simplex virus 1 envelope proteins and blocks virus maturation. Adv Virol **2015**:687162.

140. **Yamamoto N**, **Yang R**, **Yoshinaka Y**, **Amari S**, **Nakano T**, **Cinatl J**, **Rabenau H**, **Doerr HW**, **Hunsmann G**, **Otaka A**, **Tamamura H**, **Fujii N**, **Yamamoto N**. 2004. HIV protease inhibitor nelfinavir inhibits replication of SARS-associated coronavirus. Biochem. Biophys. Res. Commun. **318**:719–725.

141. **Toma S**, **Yamashiro T**, **Arakaki S**, **Shiroma J**, **Maeshiro T**, **Hibiya K**, **Sakamoto N**, **Kinjo F**, **Tateyama M**, **Fujita J**. 2009. Inhibition of intracellular hepatitis C virus replication by nelfinavir and synergistic effect with interferon-alpha. J Viral Hepat **16**:506–512.

142. **Johnson DC**, **Spear PG**. 1983. O-linked oligosaccharides are acquired by herpes simplex virus glycoproteins in the Golgi apparatus. Cell **32**:987–997.

143. **Guan M**, **Fousek K**, **Jiang C**, **Guo S**, **Synold T**, **Xi B**, **Shih C-C**, **Chow WA**. 2011. Nelfinavir induces liposarcoma apoptosis through inhibition of regulated intramembrane proteolysis of SREBP-1 and ATF6. Clin. Cancer Res. **17**:1796–1806.

144. **Guan M**, **Fousek K**, **Chow WA**. 2012. Nelfinavir inhibits regulated intramembrane proteolysis of sterol regulatory element binding protein-1 and activating transcription factor 6 in castration-resistant prostate cancer. FEBS J. **279**:2399–2411.

145. **Guan M**, **Su L**, **Yuan Y-C**, **Li H**, **Chow WA**. 2015. Nelfinavir and nelfinavir analogs block site-2 protease cleavage to inhibit castration-resistant prostate cancer. Sci. Rep. **5**:9698.

146. **Chow WA**, **Guo S**, **Valdes-Albini F**. 2006. Nelfinavir induces liposarcoma apoptosis and cell cycle arrest by upregulating sterol regulatory element binding protein-1. Anticancer Drugs **17**:891–903.

147. **Caron M**, **Auclair M**, **Sterlingot H**, **Kornprobst M**, **Capeau J**. 2003. Some HIV protease inhibitors alter lamin A/C maturation and stability, SREBP-1 nuclear localization and adipocyte differentiation. AIDS **17**:2437–2444.

148. **Yang Y**, **Ikezoe T**, **Takeuchi T**, **Adachi Y**, **Ohtsuki Y**, **Takeuchi S**, **Koeffler HP**, **Taguchi H**. 2005. HIV-1 protease inhibitor induces growth arrest and apoptosis of human prostate cancer LNCaP cells in vitro and in vivo in conjunction with blockade of androgen receptor STAT3 and AKT signaling. Cancer Sci. **96**:425–433.

149. **Gills JJ**, **Lopiccolo J**, **Tsurutani J**, **Shoemaker RH**, **Best CJM**, **Abu-Asab MS**, **Borojerdi J**, **Warfel NA**, **Gardner ER**, **Danish M**, **Hollander MC**, **Kawabata S**, **Tsokos M**, **Figg WD**, **Steeg PS**, **Dennis PA**. 2007. Nelfinavir, A lead HIV protease inhibitor, is a broad-spectrum, anticancer agent that induces endoplasmic reticulum stress, autophagy, and apoptosis in vitro and in vivo. Clin. Cancer Res. **13**:5183–5194.

150. **Koltai T**. 2015. Nelfinavir and other protease inhibitors in cancer: mechanisms involved in anticancer activity. [version 2; peer review: 2 approved]. F1000Res. **4**:9.

151. **Brüning A**, **Gingelmaier A**, **Friese K**, **Mylonas I**. 2010. New prospects for nelfinavir in non-HIV-related diseases. Curr Mol Pharmacol **3**:91–97.

152. **Shim JS**, **Liu JO**. 2014. Recent advances in drug repositioning for the discovery of new anticancer drugs. Int. J. Biol. Sci. **10**:654–663.

153. **Bernstein WB**, **Dennis PA**. 2008. Repositioning HIV protease inhibitors as cancer therapeutics. Curr Opin HIV AIDS **3**:666–675.

154. **Chow WA**, **Jiang C**, **Guan M**. 2009. Anti-HIV drugs for cancer therapeutics: back to the future? Lancet Oncol. **10**:61–71.

155. **Gantt S**, **Casper C**, **Ambinder RF**. 2013. Insights into the broad cellular effects of nelfinavir and the HIV protease inhibitors supporting their role in cancer treatment and prevention. Curr Opin Oncol **25**:495–502.

156. **Tollefson AE**, **Ying B**, **Spencer JF**, **Sagartz JE**, **Wold WSM**, **Toth K**. 2017. Pathology in Permissive Syrian Hamsters after Infection with Species C Human Adenovirus (HAdV-C) Is the Result of Virus Replication: HAdV-C6 Replicates More and Causes More Pathology than HAdV-

Antimicrobial Agents and Chemotherapy
AAC
Antimicrobial Agents and Chemotherapy
Downloaded from http://aac.asm.org/ on July 13, 2020 by guest

Accepted Manuscript Posted Online

C5. J. Virol. **91**.

157. **Radke JR**, **Yong SL**, **Cook JL**. 2016. Low-Level Expression of the E1B 20-Kilodalton Protein by Adenovirus 14p1 Enhances Viral Immunopathogenesis. J. Virol. **90**:497–505.

158. **Andriasyan V**, **Yakimovich A**, **Georgi F**, **Petkidis A**, **Witte R**, **Puntener D**, **Greber UF**. 2019. Deep learning of virus infections reveals mechanics of lytic cells. BioRxiv. DOI: https://doi.org/10.1101/798074

159. **Zou A**, **Atencio I**, **Huang W-M**, **Horn M**, **Ramachandra M**. 2004. Overexpression of adenovirus E3-11.6K protein induces cell killing by both caspase-dependent and caspase-independent mechanisms. Virology **326**:240–249.

160. **Yun C-O**, **Kim E**, **Koo T**, **Kim H**, **Lee Y**, **Kim J-H**. 2005. ADP-overexpressing adenovirus elicits enhanced cytopathic effect by induction of apoptosis. Cancer Gene Ther **12**:61–71.

161. **Davison AJ**, **Benkő M**, **Harrach B**. 2003. Genetic content and evolution of adenoviruses. J. Gen. Virol. **84**:2895–2908.

162. **Hausmann J**, **Ortmann D**, **Witt E**, **Veit M**, **Seidel W**. 1998. Adenovirus death protein, a transmembrane protein encoded in the E3 region, is palmitoylated at the cytoplasmic tail. Virology **244**:343–351.

163. **Veit M**. 2012. Palmitoylation of virus proteins. Biol. Cell **104**:493–515.

164. **Blaskovic S**, **Blanc M**, **van der Goot FG**. 2013. What does S-palmitoylation do to membrane proteins? FEBS J. **280**:2766–2774.

165. **Longer M**, **Shetty B**, **Zamansky I**, **Tyle P**. 1995. Preformulation studies of a novel HIV protease inhibitor, AG1343. J. Pharm. Sci. **84**:1090–1093.

166. **Tetko IV**, **Gasteiger J**, **Todeschini R**, **Mauri A**, **Livingstone D**, **Ertl P**, **Palyulin VA**, **Radchenko EV**, **Zefirov NS**, **Makarenko AS**, **Tanchuk VY**, **Prokopenko VV**. 2005. Virtual computational chemistry laboratory--design and description. J. Comput. Aided Mol. Des. **19**:453–463.

167. **Jurgeit A**, **McDowell R**, **Moese S**, **Meldrum E**, **Schwendener R**, **Greber UF**. 2012. Niclosamide is a proton carrier and targets acidic endosomes with broad antiviral effects. PLoS Pathog. **8**:e1002976.

168. **Fonseca BD**, **Diering GH**, **Bidinosti MA**, **Dalal K**, **Alain T**, **Balgi AD**, **Forestieri R**, **Nodwell M**, **Rajadurai CV**, **Gunaratnam C**, **Tee AR**, **Duong F**, **Andersen RJ**, **Orlowski J**, **Numata M**, **Sonenberg N**, **Roberge M**. 2012. Structure-activity analysis of niclosamide reveals potential role for cytoplasmic pH in control of mammalian target of rapamycin complex 1 (mTORC1) signaling. J. Biol. Chem. **287**:17530–17545.

169. **Baker AT**, **Greenshields-Watson A**, **Coughlan L**, **Davies JA**, **Uusi-Kerttula H**, **Cole DK**, **Rizkallah PJ**, **Parker AL**. 2019. Diversity within the adenovirus fiber knob hypervariable loops influences primary receptor interactions. Nat. Commun. **10**:741.

170. **Uchino J**, **Curiel DT**, **Ugai H**. 2014. Species D human adenovirus type 9 exhibits better virus-spread ability for antitumor efficacy among alternative serotypes. PLoS One **9**:e87342.

171. **Chen CY**, **Senac JS**, **Weaver EA**, **May SM**, **Jelinek DF**, **Greipp P**, **Witzig T**, **Barry MA**. 2011. Species D adenoviruses as oncolytics against B-cell cancers. Clin. Cancer Res. **17**:6712–6722.

172. **Galluzzi L**, **Vitale I**, **Aaronson SA**, **Abrams JM**, **Adam D**, **Agostinis P**, **Alnemri ES**, **Altucci L**, **Amelio I**, **Andrews DW**, **Annicchiarico-Petruzzelli M**, **Antonov AV**, **Arama E**, **Baehrecke EH**, **Barlev NA**, **Bazan NG**, **Bernassola F**, **Bertrand MJM**, **Bianchi K**, **Blagosklonny MV**, **Blomgren K**, **Borner C**, **Boya P**, **Brenner C**, **Campanella M**, **Candi E**, **Carmona-Gutierrez D**, **Cecconi F**, **Chan FK-M**, **Chandel NS**, **Cheng EH**, **Chipuk JE**, **Cidlowski JA**, **Ciechanover A**, **Cohen GM**, **Conrad M**, **Cubillos-Ruiz JR**, **Czabotar PE**, **D'Angiolella V**, **Dawson TM**, **Dawson VL**, **De Laurenzi V**, **De Maria R**, **Debatin K-M**, **DeBerardinis RJ**, **Deshmukh M**, **Di Daniele N**, **Di Virgilio F**, **Dixit VM**, **Dixon SJ**, **Duckett CS**, **Dynlacht BD**, **El-Deiry WS**, **Elrod JW**, **Fimia GM**, **Fulda S**, **García-Sáez AJ**, **Garg AD**, **Garrido C**, **Gavathiotis E**, **Golstein P**, **Gottlieb E**, **Green DR**, **Greene LA**, **Gronemeyer H**, **Gross A**, **Hajnoczky G**, **Hardwick JM**, **Harris IS**, **Hengartner MO**, **Hetz C**, **Ichijo H**, **Jäättelä M**, **Joseph B**, **Jost PJ**, **Juin PP**, **Kaiser WJ**, **Karin M**, **Kaufmann T**, **Kepp O**, **Kimchi A**, **Kitsis RN**, **Klionsky DJ**, **Knight RA**, **Kumar S**, **Lee SW**, **Lemasters JJ**, **Levine B**, **Linkermann A**, **Lipton SA**, **Lockshin RA**, **López-Otín C**, **Lowe SW**, **Luedde T**, **Lugli**

Downloaded from http://aac.asm.org/ on July 13, 2020 by guest

Antimicrobial Agents and Chemotherapy

AAC

Antimicrobial Agents and Chemotherapy

Accepted Manuscript Posted Online

E, **MacFarlane M**, **Madeo F**, **Malewicz M**, **Malorni W**, **Manic G**, **Marine J-C**, **Martin SJ**, **Martinou J-C**, **Medema JP**, **Mehlen P**, **Meier P**, **Melino S**, **Miao EA**, **Molkentin JD**, **Moll UM**, **Muñoz-Pinedo C**, **Nagata S**, **Nuñez G**, **Oberst A**, **Oren M**, **Overholtzer M**, **Pagano M**, **Panaretakis T**, **Pasparakis M**, **Penninger JM**, **Pereira DM**, **Pervaiz S**, **Peter ME**, **Piacentini M**, **Pinton P**, **Prehn JHM**, **Puthalakath H**, **Rabinovich GA**, **Rehm M**, **Rizzuto R**, **Rodrigues CMP**, **Rubinsztein DC**, **Rudel T**, **Ryan KM**, **Sayan E**, **Scorrano L**, **Shao F**, **Shi Y**, **Silke J**, **Simon H-U**, **Sistigu A**, **Stockwell BR**, **Strasser A**, **Szabadkai G**, **Tait SWG**, **Tang D**, **Tavernarakis N**, **Thorburn A**, **Tsujimoto Y**, **Turk B**, **Vanden Berghe T**, **Vandenabeele P**, **Vander Heiden MG**, **Villunger A**, **Virgin HW**, **Vousden KH**, **Vucic D**, **Wagner EF**, **Walczak H**, **Wallach D**, **Wang Y**, **Wells JA**, **Wood W**, **Yuan J**, **Zakeri Z**, **Zhivotovsky B**, **Zitvogel L**, **Melino G**, **Kroemer G**. 2018. Molecular mechanisms of cell death: recommendations of the Nomenclature Committee on Cell Death 2018. Cell Death Differ. **25**:486–541.

173. **Dziengelewski C**, **Rodrigue M-A**, **Caillier A**, **Jacquet K**, **Boulanger M-C**, **Bergeman J**, **Fuchs M**, **Lambert H**, **Laprise P**, **Richard DE**, **Bordeleau F**, **Huot M-É**, **Lavoie JN**. 2020. Adenoviral protein E4orf4 interacts with the polarity protein Par3 to induce nuclear rupture and tumor cell death. J. Cell Biol. **219**.

174. **Verboon JM, Nakamura M, Davidson KA, Decker JR, Nandakumar V, Parkhurst SM. 2020. Wash and the wash regulatory complex function in nuclear envelope budding. J Cell Sci doi:10.1242/jcs.243576.**

175. **Hagen C**, **Dent KC**, **Zeev-Ben-Mordehai T**, **Grange M**, **Bosse JB**, **Whittle C**, **Klupp BG**, **Siebert CA**, **Vasishtan D**, **Bäuerlein FJB**, **Cheleski J**, **Werner S**, **Guttmann P**, **Rehbein S**, **Henzler K**, **Demmerle J**, **Adler B**, **Koszinowski U**, **Schermelleh L**, **Schneider G**, **Enquist LW**, **Plitzko JM**, **Mettenleiter TC**, **Grünewald K**. 2015. Structural basis of vesicle formation at the inner nuclear membrane. Cell **163**:1692–1701.

176. **Lippincott-Schwartz J**, **Freed EO**, **van Engelenburg SB**. 2017. A Consensus View of ESCRT-Mediated Human Immunodeficiency Virus Type 1 Abscission. Annu. Rev. Virol. **4**:309–325.

177. **Feng Z**, **Hensley L**, **McKnight KL**, **Hu F**, **Madden V**, **Ping L**, **Jeong S-H**, **Walker C**, **Lanford RE**, **Lemon SM**. 2013. A pathogenic picornavirus acquires an envelope by hijacking cellular membranes. Nature **496**:367–371.

178. **Hurley JH**. 2015. ESCRTs are everywhere. EMBO J. **34**:2398–2407.

179. **Murali VK**, **Ornelles DA**, **Gooding LR**, **Wilms HT**, **Huang W**, **Tollefson AE**, **Wold WSM**, **Garnett-Benson C**. 2014. Adenovirus death protein (ADP) is required for lytic infection of human lymphocytes. J. Virol. **88**:903–912.

180. **Garnett CT**, **Erdman D**, **Xu W**, **Gooding LR**. 2002. Prevalence and quantitation of species C adenovirus DNA in human mucosal lymphocytes. J. Virol. **76**:10608–10616.

181. **Zheng Y**, **Stamminger T**, **Hearing P**. 2016. E2f/rb family proteins mediate interferon induced repression of adenovirus immediate early transcription to promote persistent viral infection. PLoS Pathog. **12**:e1005415.

182. **Kosulin K**, **Geiger E**, **Vécsei A**, **Huber WD**, **Rauch M**, **Brenner E**, **Wrba F**, **Hammer K**, **Innerhofer A**, **Pötschger U**, **Lawitschka A**, **Matthes-Leodolter S**, **Fritsch G**, **Lion T**. 2016. Persistence and reactivation of human adenoviruses in the gastrointestinal tract. Clin. Microbiol. Infect. **22**:381.e1-381.e8.

183. **Hiwarkar P**, **Kosulin K**, **Cesaro S**, **Mikulska M**, **Styczynski J**, **Wynn R**, **Lion T**. 2018. Management of adenovirus infection in patients after haematopoietic stem cell transplantation: State-of-the-art and real-life current approach: A position statement on behalf of the Infectious Diseases Working Party of the European Society of Blood and Marrow Transplantation. Rev Med Virol **28**:e1980.

Downloaded from http://aac.asm.org/ on July 13, 2020 by guest

Antimicrobial Agents and Chemotherapy
AAC
Antimicrobial Agents and Chemotherapy

Accepted Manuscript Posted Online

Antimicrobial Agents and Chemotherapy

AAC

Antimicrobial Agents and Chemotherapy

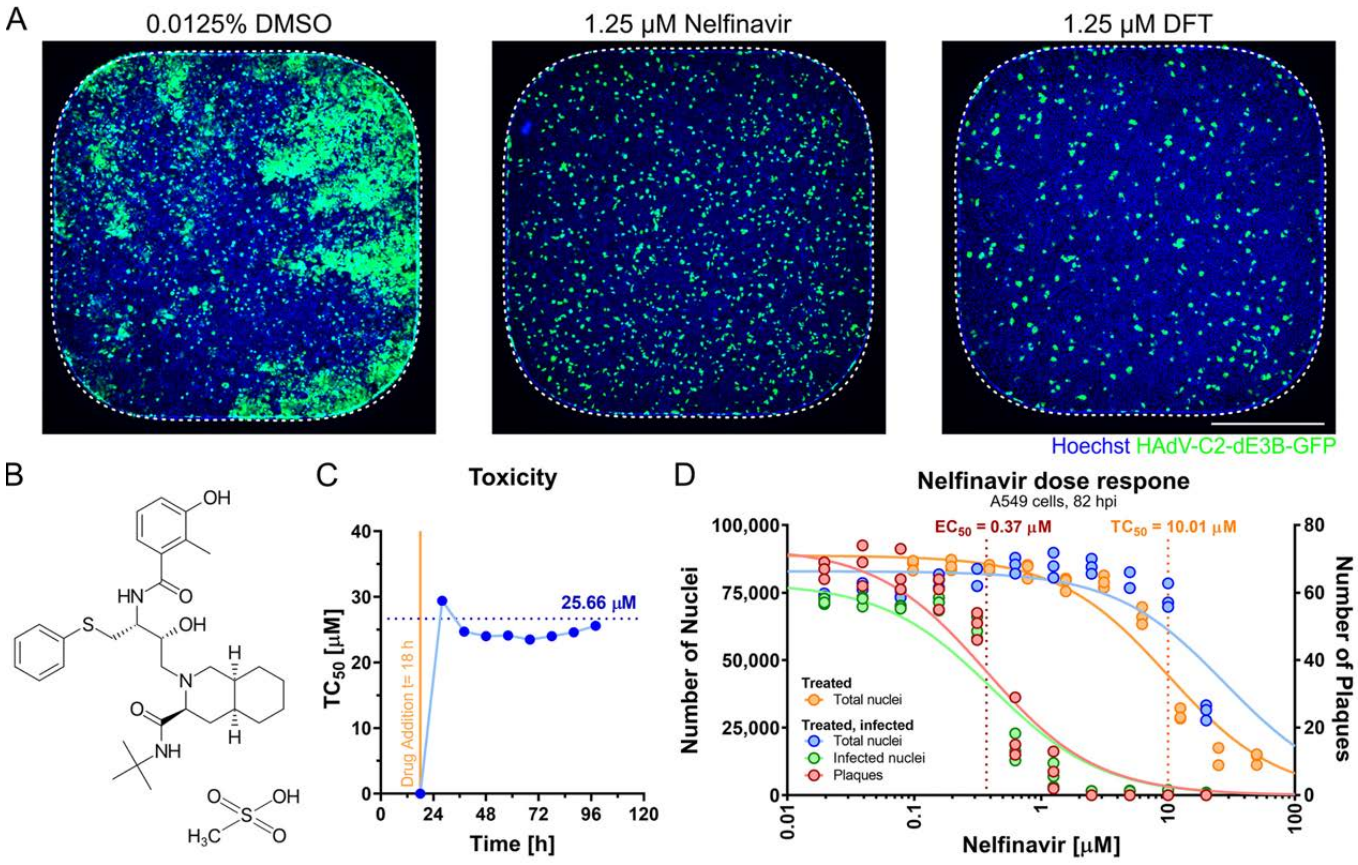

Downloaded from http://aac.asm.org/ on July 13, 2020 by guest

Accepted Manuscript Posted Online

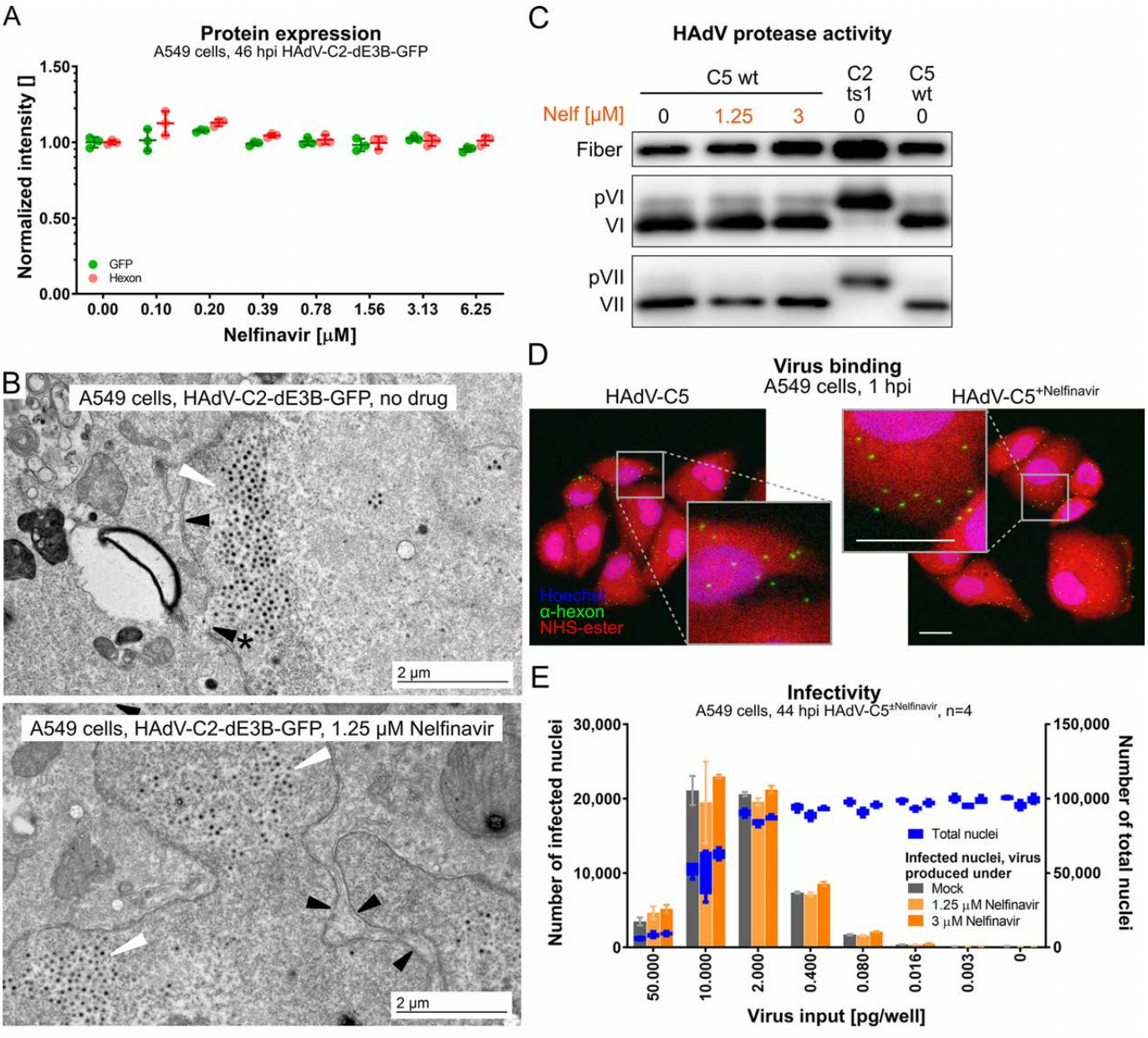

Downloaded from http://aac.asm.org/ on July 13, 2020 by guest

Antimicrobial Agents and Chemotherapy
AAC
Antimicrobial Agents and Chemotherapy

Accepted Manuscript Posted Online

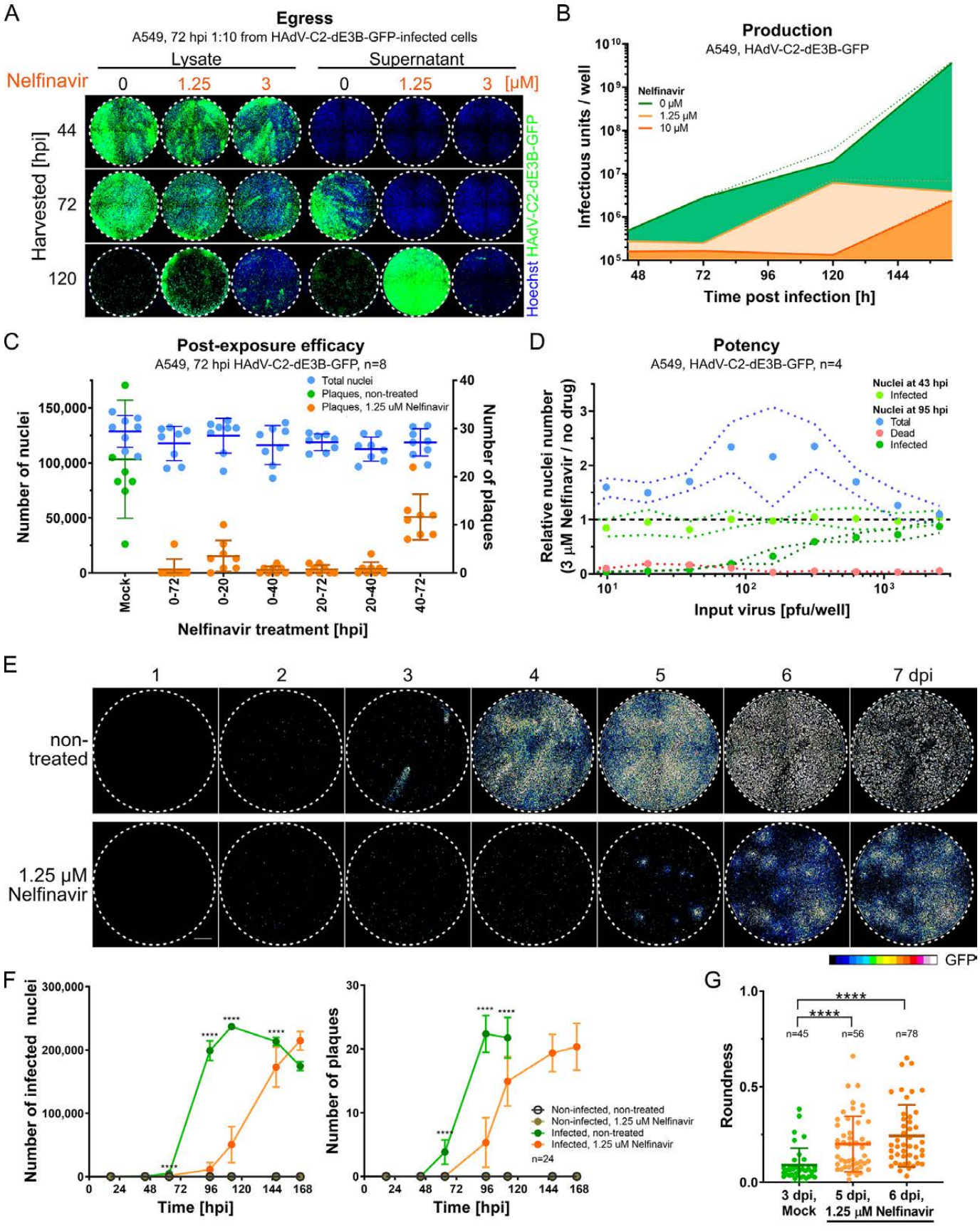

Downloaded from http://aac.asm.org/ on July 13, 2020 by guest

AAC
Antimicrobial Agents and Chemotherapy
Antimicrobial Agents and Chemotherapy

Accepted Manuscript Posted Online

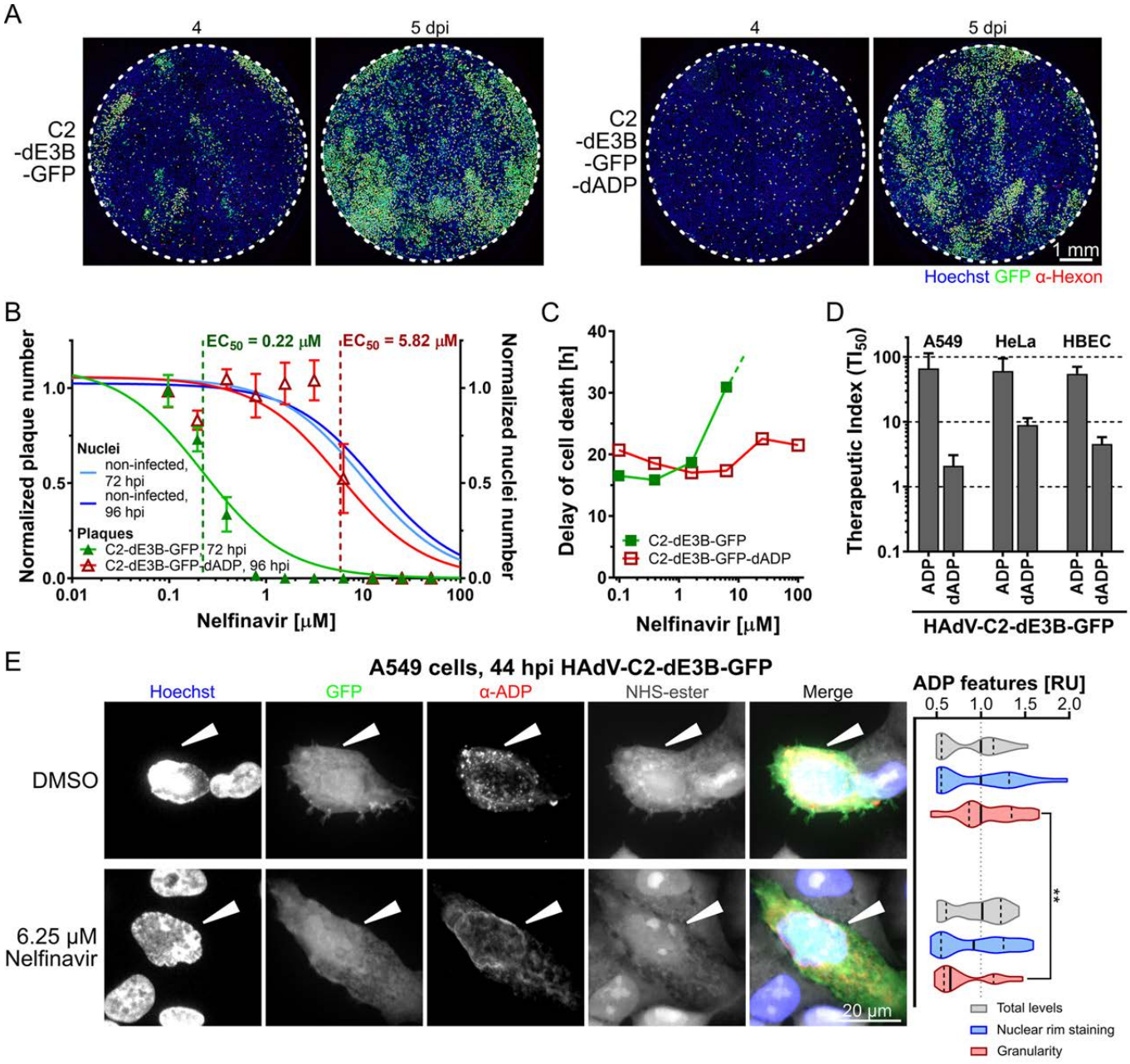

Downloaded from http://aac.asm.org/ on July 13, 2020 by guest

AAC
Antimicrobial Agents and Chemotherapy

Antimicrobial Agents and Chemotherapy

Accepted Manuscript Posted Online

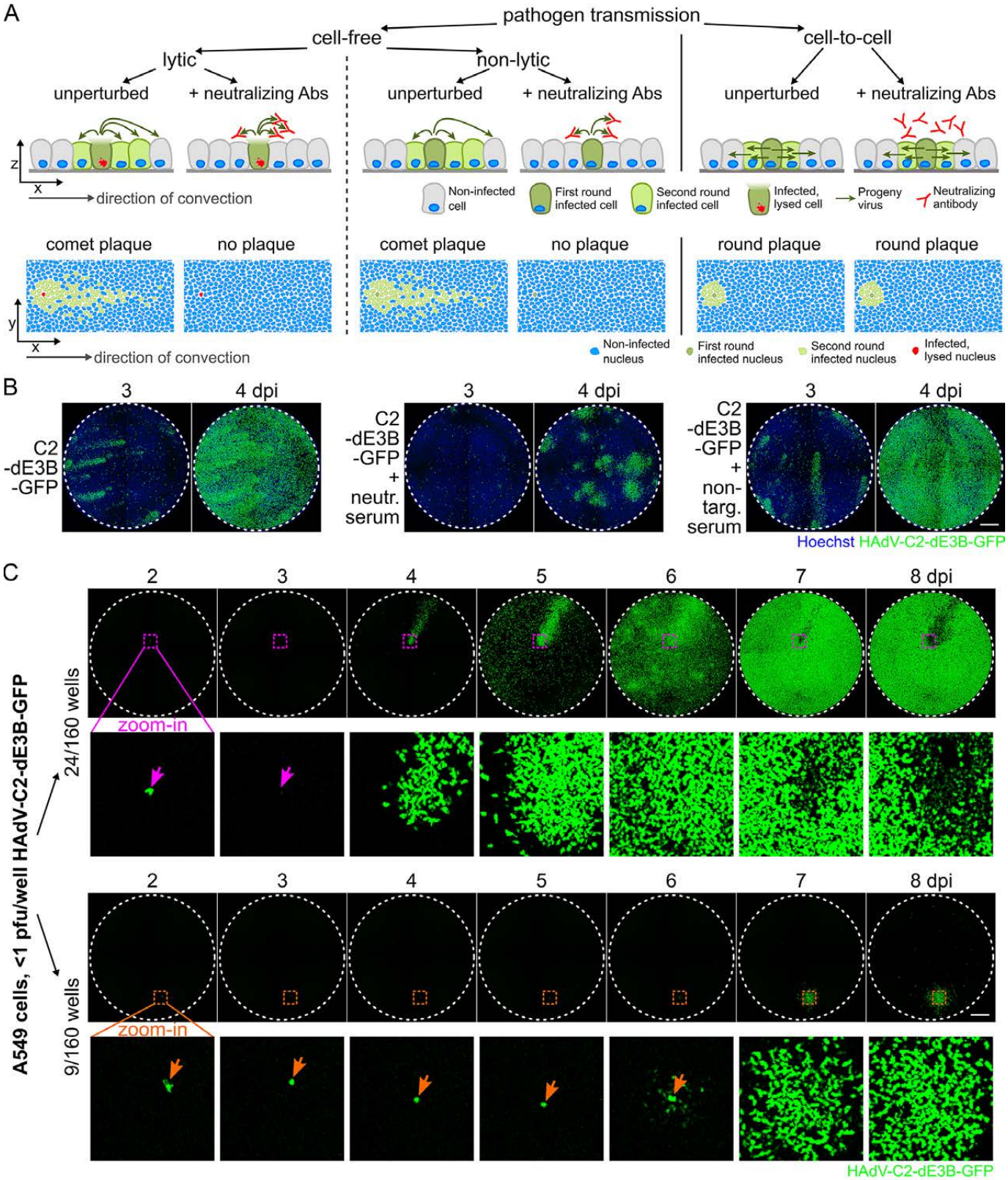

Downloaded from http://aac.asm.org/ on July 13, 2020 by guest

Antimicrobial Agents and Chemotherapy

AAC

Antimicrobial Agents and Chemotherapy

Accepted Manuscript Posted Online

Antimicrobial Agents and Chemotherapy

AAC

Antimicrobial Agents and Chemotherapy

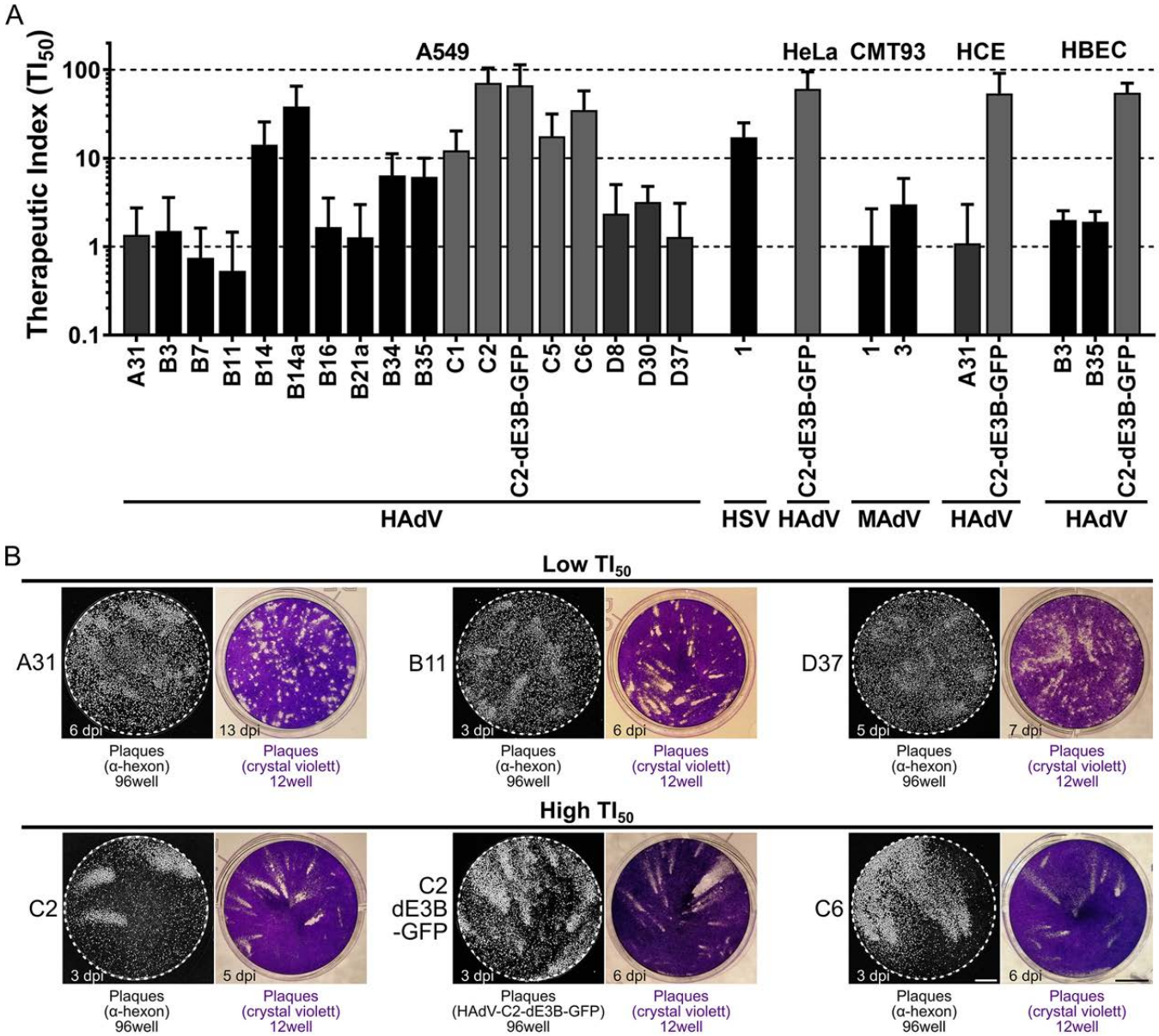

Downloaded from http://aac.asm.org/ on July 13, 2020 by guest